cytosine in the CGG/CGG triad was free from the G–C base pairing upon **NC** binding. We examined the reaction of **NC**-bound CGG/CGG triad with hydroxylamine. Cytosines in the single-stranded regions and in the mismatched base pairs efficiently reacted with two molecules of hydroxylamine at the C4 and C6 positions, whereas those in the G–C base pair in a duplex were not susceptible to the addition of hydroxylamine. The cytosine modified with hydroxylamine underwent degradation on heating with piperidine, eventually leading to strand cleavage.[13]

The reaction of 11-mer self-complementary 5′-d(TCAA CGG TTGA)-3′ (**1**) with hydroxylamine was monitored by reversed-phase HPLC (Figure 3). The duplex of **1**

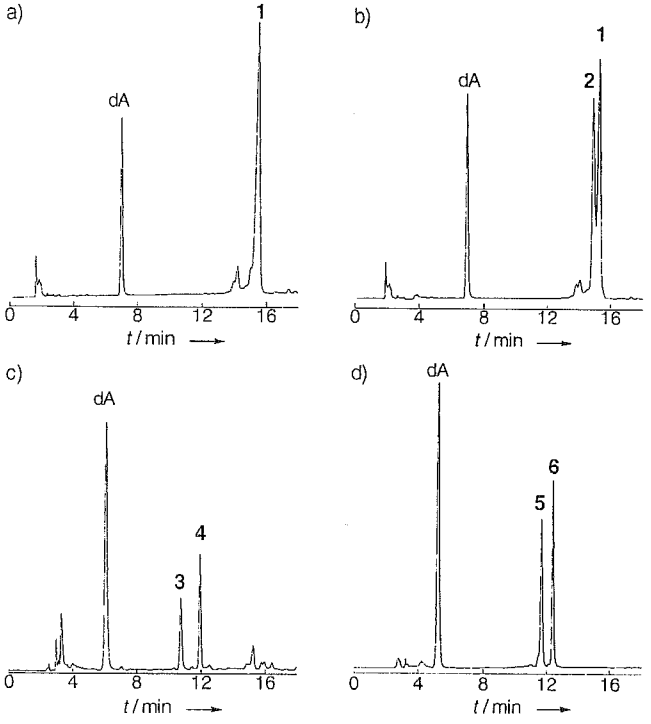

Figure 3. HPLC profiles for the hydroxylamine-induced cleavage at the cytosine moiety in the CGG/CGG triad. The 11-mer self-complementary oligomer 5′-d(TCAA CGG TTGA)-3′ (**1**) (13 μM as a duplex) in NaCl (100 mM) was treated with hydroxylamine (2.8 M, pH 6.0) in the a) absence and b) presence of **NC** (40 μM) at 0 °C for 12 h. c) Product **2** was isolated and treated with piperidine at 90 °C for 30 min. d) Products **3** and **4** were treated with alkaline phosphatase at 37 °C for 2 h. Deoxyadenosine (dA) was added as an internal standard.

(13 μM) was not reactive toward hydroxylamine (2.8 M, pH 6.0) at 0 °C for 12 h, whereas a new product **2** was produced in the presence of **NC** (40 μM). A prolonged reaction time (≈24 h) resulted in 70% consumption of **1** without the formation of any major by-products (see the Supporting Information), which suggests that both strands of **1** duplex reacted with hydroxylamine and produced **2**. MALDI-TOF MS showed that product **2** was the adduct of **1** with two molecules of hydroxylamine (*m/z*: found 3406.06, calcd 3403.62; see Scheme 1 and the Supporting Information).[13] After isolation by HPLC, product **2** was treated with piperidine at 90 °C for 30 min to give products **3** and **4**. The

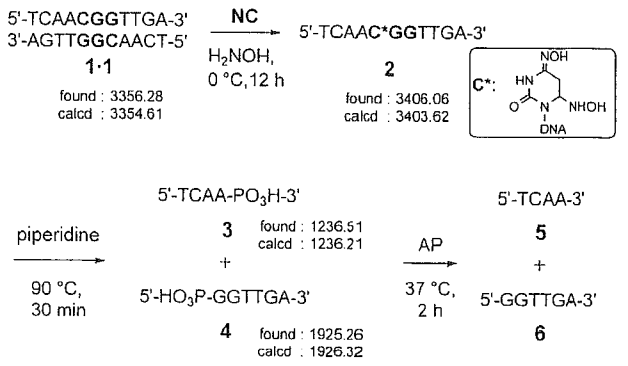

Scheme 1. Hydroxylamine-induced cleavage at cytosine in the **NC**-bound CGG/CGG triad. AP = alkaline phosphatase.

MALDI-TOF mass spectra showed that **3** was the oligomer 5′-d(TCAA)-PO_3H-3′ (*m/z*: found 1236.51, calcd 1236.21), whereas **4** was the oligomer 5′-HO_3P-d(GGTTGA)-3′ (*m/z*: found 1925.26, calcd 1926.32). The phosphorylated termini of **3** and **4** were removed by treatment with alkaline phosphatase to give 5′-d(TCAA)-3′ (**5**) and 5′-d(GGTTGA)-3′ (**6**), respectively. The oligomers **5** and **6** showed the same retention times as authentic oligomers, as observed by co-injection in reversed-phase HPLC. These HPLC analyses clarified that the cytosine in the CGG/CGG triad in **1** duplex became susceptible to the hydroxylamine upon binding with **NC**. The **1** duplex contained two kinds of cytosine, one in the CGG/CGG triad and the other in 5′-TCA-3′/5′-TGA-3′. The cytosine in the latter sequence was insensitive to hydroxylamine, regardless of the presence of **NC**. These results showed that the binding of **NC** to the CGG/CGG triad made the cytosine free from the base pairing to the guanine moiety in the opposite strand.

CSI-TOF MS measurements suggested that the 2:1 **NC**-CGG/CGG complex, which was confirmed for an oligomer duplex, was also produced in the $(CGG)_n$ repeat. CSI-TOF MS of $d(CGG)_{10}$ with **NC** showed the ions corresponding to $[d(CGG)_{10}+6\mathbf{NC}]^{6-}$ and $[d(CGG)_{10}+6\mathbf{NC}]^{7-}$, which suggests the formation of the 2:1 **NC**-CGG/CGG triad complex in the $d(CGG)_{10}$ repeat (see the Supporting Information). In addition, a large conformational change of $d(CGG)_{10}$ was observed in CD measurements upon binding with **NC** (see the Supporting Information), which supports the formation of a hairpin structure, as observed in the binding of **NA** to $d(CAG)_{10}$.[7]

In summary, the data presented herein have shown that 1) **NC** is the first molecule to bind to the CGG/CGG triad, and 2) the cytosine in the triad is free from hydrogen bonding to the guanine moiety upon **NC** binding. It is suggested that the 2:1 **NC**-CGG/CGG complex is produced in the hairpin structure of the $d(CGG)_n$ repeat, which is proposed to form in the replication leading to the repeat expansion. From the structural viewpoint, the **NC**-bound CGG repeats are particularly interesting. Base flipping as a result of the disruption of base pairing is one of the mechanisms for the repair enzyme to recognize the damaged bases and mismatched base pairs.[14–17] Therefore, **NC** could be a useful molecule for studying not only the repeat expansion mechanism, but also

the nucleobase–ligand interactions on the biologically important repeat sequence.

Received: June 30, 2005
Revised: August 20, 2005
Published online: October 17, 2005

Keywords: DNA cleavage · mass spectrometry · nucleotides

[1] S. T. Warren, C. T. Ashley, *Annu. Rev. Neurosci.* **1995**, *18*, 77–99.
[2] R. D. Wells, S. T. Warren, *Genetic Instabilities and Hereditary Neurological Diseases*, Academic Press, New York, **1998**.
[3] A. Brussino, C. Gellera, A. Saluto, C. Mariotti, C. Arduino, B. Castellotti, M. Camerlingo, V. de Angelis, L. Orsi, P. Tosca, N. Migone, F. Taroni, A. Brusco, *Neurology* **2005**, *64*, 145–147.
[4] A. M. Gacy, G. Goellner, N. Juranic, S. Macura, C. T. McMurray, *Cell* **1995**, *81*, 533–540.
[5] K. Ohshima, R. D. Wells, *J. Biol. Chem.* **1997**, *272*, 16798–16806.
[6] A. M. Paiva, R. D. Sheardy, *J. Am. Chem. Soc.* **2005**, *127*, 5581–5585.
[7] K. Nakatani, S. Hagihara, Y. Goto, A. Kobori, M. Hagihara, G. Hayashi, M. Kyo, M. Nomura, M. Mishima, C. Kojima, *Nat. Chem. Biol.* **2005**, *1*, 39–43.
[8] K. Nakatani, S. Sando, I. Saito, *Nat. Biotechnol.* **2001**, *19*, 51–55.
[9] K. Nakatani, S. Sando, H. Kumasawa, J. Kikuchi, I. Saito, *J. Am. Chem. Soc.* **2001**, *123*, 12650–12657.
[10] K. Nakatani, S. Sando, I. Saito, *Bioorg. Med. Chem.* **2001**, *9*, 2381–2385.
[11] T. Peng, T. Murase, Y. Goto, A. Kobori, K. Nakatani, *Bioorg. Med. Chem. Lett.* **2005**, *15*, 259–262.
[12] K. Yamaguchi, *J. Mass Spectrom.* **2003**, *38*, 473–490.
[13] B. H. Johnston, *Methods Enzymol.* **1992**, *212*, 180–194.
[14] R. J. Roberts, X. Chen, *Annu. Rev. Biochem.* **1998**, *67*, 181–198.
[15] E. Seibert, J. B. A. Ross, R. Osman, *J. Mol. Biol.* **2003**, *330*, 687–703.
[16] D. S. Daniels, T. T. Woo, K. X. Luu, D. M. Noll, N. D. Clarke, A. E. Pegg, J. A. Tainer, *Nat. Struct. Mol. Biol.* **2004**, *11*, 714–720.
[17] C. Cao, Y. L. Jiang, J. T. Stivers, F. Song, *Nat. Struct. Mol. Biol.* **2004**, *11*, 1230–1236.

Molecular labeling of the CGG trinucleotide repeat

Tao Peng and Kazuhiko Nakatani*

The Institute of Scientific and Industrial Research, Osaka University, Ibaraki 567-0047, Japan

ABSTRACT

The new molecular ligand naphthyridine carbamate dimer (NC), possessing 2-amino-1,8-naphthyridines and a carbamate linker, specially binds to guanine–guanine (G–G) mismatch in duplex DNA. The results of T_m measurements showed that NC selectively bound to CGG/CGG triad with high ΔT_m of 23.1 °C. The exclusive stoichiometry 2:1 of the complex of NC with CGG/CGG triad, obtained by the measurements of cold spray ionization time-of-flight mass spectrometry (CSI-TOF MS), showed that NC bound to CGG/CGG triad strongly with two molecules.

INTRODUCTION

Fragile X syndrome is the most commonly inherited form of mental retardation. The fragile X gene (FMR1) was characterized and found to contain a tandem repeated trinucleotide sequence (CGG) near its 5' end.[1] The molecular basis for the (CGG)n expansion is proposed to involve the formation of a metastable hairpin structure in a leading strand during the replication.[2] The hairpin structure of (CGG)n is consisted of continued 5'-CGG-3'/5'-CGG-3' triads, where a G-G mismatch was flanked by two C-G base pairs. We have synthesized several small molecular ligands which could bind to the particular triad sequence to molecularly label the (CGG)n repeat sequence.[3,4] We here report NC strongly binds to the CGG/CGG triad.

RESULTS AND DISCUSSION

NC was synthesized as shown in Scheme 1. Firstly, *N*-Boc-Di-propanolamine was reacted with *N,N'*-disuccinimidyl carbonate (DSC) in dry acetonitrile to produce carbonate **2**.[5] Then **2** was reacted with 2-amino-7-methyl-1,8-naphthyridine to afford Boc-protected **NC**. At last, deprotection by hydrogen chloride in ethyl acetate gave hydrochloride salt of **NC**.

After synthesized the target compound **NC**, the selective binding of **NC** to the G-G mismatch was studied. The assay was carried out by measuring the melting temperature (T_m) of 13-mer duplex 5'-d(GCTAA **xGz** AATGA)-3'/5'-d(TCATT **wGy** TTAGC)-3' containing a G-G mismatch flanked by any combination of Watson-Crick base pairs (Table 1). The ΔT_m values obtained for these sequences were highly dependent on the base pairs flanking the G-G mismatch. The largest ΔT_m value of 23.1 °C was recorded for 5'-**cGg**-3'/5'-**cGg**-3'

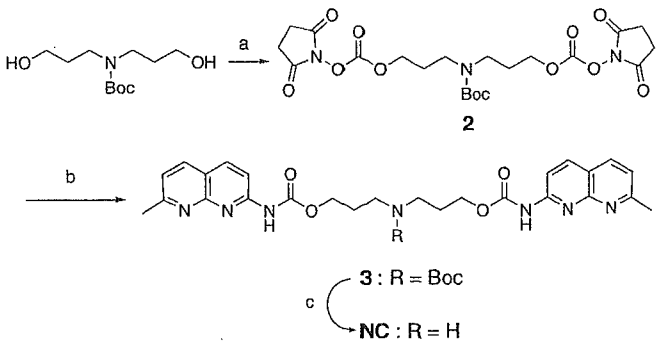

Scheme 1. Reagents and conditions: (a) *N,N'*-disuccinimidyl carbonate, CH_3CN, Et_3N; (b) 2-amino-7-methyl-1,8-naphthyridine, CH_2Cl_2, Et_3N, 49% for 2 steps; (c) HCl, AcOEt, $CHCl_3$, quantitative.

mismatch, whereas only small ΔT_m value was obtained for GGC/GGC (6.1 °C) and GGT/AGC (5.6 °C). **NC**-binding increased the T_m of CGC/GGG and CGA/TGG by 10.7 °C and 12.6 °C, respectively, suggesting that 5' side C and /or 3' side G to the G-G mismatch would be important for **NC**-binding to the G-G mismatch. While large T_m increase was observed for AGT/AGT and TGA/TGA, it is due to the low T_m value of the oligomer alone.

Table 1. Melting Temperature (T_m/°C) of the 13-mer Duplex Containing a G-G mismatch in Different Flanking Sequences in the Absence and Presence of **NC** [a]

5'-GCTAAx**Gz**AATGA-3'
3'-CGATTy**Gw**TTACT-5'

5'-xGz-3'/5'-wGy-3'	T_m(–)[b]	T_m(+)[c]	ΔT_m[d]
cGg/cGg	34.1 (0.9)	57.2 (0.4)	23.1 (0.4)
cGc/gGg	38.6 (0.1)	49.3 (0.8)	10.7 (0.8)
gGc/gGc	40.4 (0.3)	47.1 (1.4)	6.7 (1.4)
cGa/tGg	31.8 (0.2)	44.4 (0.3)	12.6 (0.3)
cGt/aGg	33.6 (0.2)	44.0 (0.5)	10.4 (0.5)
gGa/tGc	34.2 (0.3)	43.4 (0.4)	9.2 (0.4)
aGt/aGt	28.7 (0.4)	41.9 (1.0)	13.2 (1.0)
aGg/cGt	31.8 (0.6)	39.9 (0.8)	8.1 (0.8)
gGt/aGc	33.7 (0.4)	39.3 (0.3)	5.6 (0.3)
tGa/tGa	17.8 (0.4)	35.9 (1.0)	18.1 (1.0)

[a] The UV-melting curve was measured for a duplex (4.5 μM) in a 10 mM sodium cacodylate buffer (pH 7.0) containing 100 mM NaCl. Temperature was increased at a rate of 1 °C/min. All measurements were taken in three times, and standard deviations are shown in the parentheses. [b] T_m values of oligomers. [c] T_m values of oligomers in the presence of **NC** (100 μM). [d] ΔT_m was calculated as a difference of T_m(+) and T_m(–).

Cold spray ionization time-of-flight mass spectrometry (CSI-TOF MS) of 11-mer self-complementary duplex 5'-d(TCAA **CGG** TTGA)-3'/5'-d(TCAA **CGG** TTGA)-3'containing the CGG/CGG triad was measured in theabsence and presence of **NC** to directly observe the **NC**-CGG/CGG complex (Figure 1). Three ions derived from the oligomer were detected without **NC**. One ion was corresponding to a 3– ion of a single stranded form ($[\mathbf{ss}]^{3-}$) (m/z, found 1118.13; calcd. 1117.19). The other two ions were detected as a 5– ion of duplexes ($[\mathbf{G\text{-}G}]^{5-}$) (found 1342.32; calcd. 1340.83) and a 4– ion of duplexes ($[\mathbf{G\text{-}G}]^{4-}$) (found 1678.07; calcd. 1676.29), respectively. In the presence of one molar equivalent of **NC**, only one new ion (found 1544.13; calcd. 1542.13) corresponding to the 5– ion of a 2:1 complex of **NC** and the duplex ($[\mathbf{G\text{-}G} + 2\mathbf{NC}]^{5-}$) appeared. The intensity of the ions of $[\mathbf{ss}]^{3-}$, $[\mathbf{G\text{-}G}]^{5-}$, and $[\mathbf{G\text{-}G}]^{4-}$ became weak at the same time. With two molar equivalents of **NC**, ions derived from free duplex were disappeared and only $[\mathbf{G\text{-}G} + 2\mathbf{NC}]^{5-}$ was detected. Under the increased concentration of **NC**, the ion corresponding to $[\mathbf{G\text{-}G} + 2\mathbf{NC}]^{5-}$ was still predominant. These results clearly showed that the binding of **NC** to the duplex containing the CGG/CGG triad proceeded in an exclusive stoichiometry of 2:1.

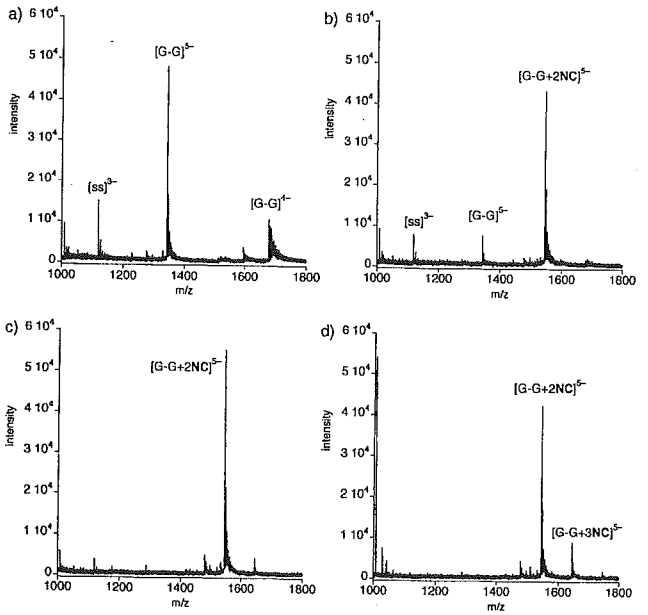

Figure 1. CSI-TOF mass spectra of 11-mer self-complementary duplex 5'-d(TCAA **CGG** TTGA)-3'/5'-d(TCAA **CGG** TTGA)-3' containing the CGG/CGG triad in the absence and presence of **NC**. Samples contained 20 μM duplex in 50% aqueous methanol and 100 mM ammonium acetate. For clarity, the range of m/z from 1000 to 1800 was shown. The sample solution was cooled at –10 °C during the injection with a flow rate of 0.5 mL/h. Key: (a) duplex only; (b) duplex with 20 μM **NC**; (c) duplex with 40 μM **NC**; (d) duplex with 60 μM **NC**.

CSI-TOF MS of $d(CGG)_{10}$ was measured in the absence and presence of **NC** (Figure 2). In the absence of **NC**, two ions corresponding to 5– ion of $d(CGG)_{10}$ ($[\mathbf{CGG}]^{5-}$) (m/z, found 1903.94; calcd. 1880.90) and 6– ion of $d(CGG)_{10}$ ($[\mathbf{CGG}]^{6-}$) (found 1572.13; calcd. 1567.25) (Figure 2a), respectively, were observed. Upon addition of six equivalents of **NC** to the duplex solution, two new ions corresponding to the 6– ion of 6:1 complex of **NC** and the $d(CGG)_{10}$ ($[\mathbf{CGG} + 6\mathbf{NC}]^{6-}$) (found 2073.37; calcd. 2070.48) and the 7– ion of 6:1 complex of **NC** and the $d(CGG)_{10}$ ($[\mathbf{CGG} + 6\mathbf{NC}]^{7-}$) (found 1776.92; calcd. 1774.55) appeared. This result clearly showed that **NC** could bind to CGG trinucleotide repeat.

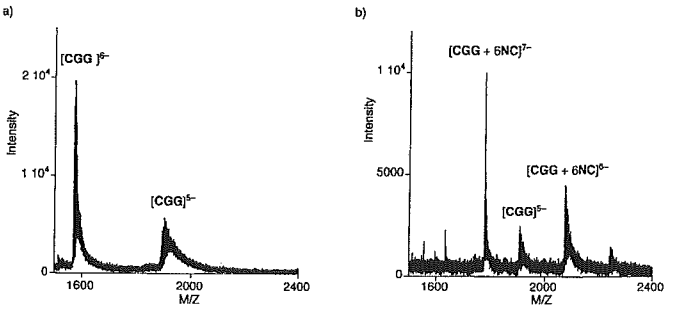

Figure 2. CSI-TOF mass spectra of $d(CGG)_{10}$ in the absence and presence of **NC**. Samples contained 20 μM duplex in 50% aqueous methanol and 100 mM ammonium acetate. For clarity, the range of m/z from 1500 to 2400 was shown. The sample solution was cooled at –10 °C during the injection with a flow rate of 0.5 mL/h. Key: (a) duplex only and (b) duplex with 120 μM **NC**.

CONCLUSION

All of the above data showed that the ligand **NC** could selectivity bind to the G-G mismatch. **NC** bound to CGG/CGG triad with an exclusive stoichiometry of 2:1 fashion. **NC** bound to CGG trinucleotide repeat could be thought as molecular label.

REFERENCES

1. Wells, R. D. and Warren, S. T. *Genetic Instabilities and Hereditary Neurological Diseases*; Academic Press: New York, 1998.
2. Gacy, A. M., Goellner, G., Juranic, N., Macura, S. and McMurray, C. T. *Cell* **1995**, *81*, 533-540.
3. Nakatani, K.; Sando, S. and Saito, I. *Nat. Biotechnol.* **2001**, *19*, 51-55.
4. Nakatani, K.; Sando, S.; Kumasawa, H.; Kikuchi, J. and Saito, I. *J. Am. Chem. Soc.* **2001**, *123*, 12650-12657.
5. Ghosh, A. K.; Duong, T. T.; McKee, S. P. and Thompson, W. J. *Tetrahedron Lett.* **1992**, *33*, 2781-2784.

Nucleic Acids Symposium Series No. 49 261–262

Application of L-DNA as a molecular tag

Gosuke Hayashi[1], Masaki Hagihara[2] and Kazuhiko Nakatani[2]

[1]Graduate School of Engineering, Kyoto University, Kyoto, 615-8246, Japan and [2]The Institute of Scientific and Industrial Research, Osaka University, Ibaraki, 567-0047, Japan

ABSTRACT

Enantiomeric DNA termed as L-DNA has unique properties. One is the ability of hybridizing to the complementary DNA as natural D-DNA. Another property is that the L-DNA could be recognized much more weakly by enzymes than D-DNA. We have focused our attention on these properties and applied L-DNA as a molecular tag. Here, we report that L-D chimera DNA is useful for PCR primers and subsequent separation and hybridization. Precise investigation revealed that in the process of PCR, L-DNA region could not be the PCR template and the polymerase extension reaction stopped at the boundary between L- and D-DNA region. As a result, L-DNA region formed like a "sticky end" and played a role of molecular tag. According to the L-DNA tag sequence, the produced L-DNA-tagged PCR products were easily separated or hybridized on the solid surface where the complementary L-DNA was pre-immobilized.

INTRODUCTION

L-DNA is an enantiomer of natural form of D-DNA. In biological systems, L-DNA and D-DNA mostly behave differently because, when L-DNA bound to proteins, sugars and nucleic acids, the produced complexes were diastereomeric to those produced from D-DNA. We have focused on the chemical properties of L-DNA and studied the application of L-DNA as a molecular tag in DNA microarray technology. DNA microarray is important tools for the biological studies. One drawback in current microarray technology is the lack of methods to directly immobilize the duplex DNA, e.g. PCR products on the array surface. We here show a chimera DNA consisting of L- and D-DNA are useful primers for PCR reaction and subsequent immobilization of duplexes on the array surface.

RESULTS AND DISCUSSION

The L-deoxynucleoside phosphoramidite units L-dT, L-dC, L-dA and L-dG were prepared according to the literatures[3, 4] (Scheme 1). The L-deoxyribose derivative **2** was synthesized from L-arabinose **1** through 8 steps. The L-deoxynucleosides were obtained by a glycosylation of appropriate nucleobase derivatives with compound **2**. After derivatization to nucleoside phosphoramidites, they were incorporated into L-D chimera oligodeoxynucleosides,

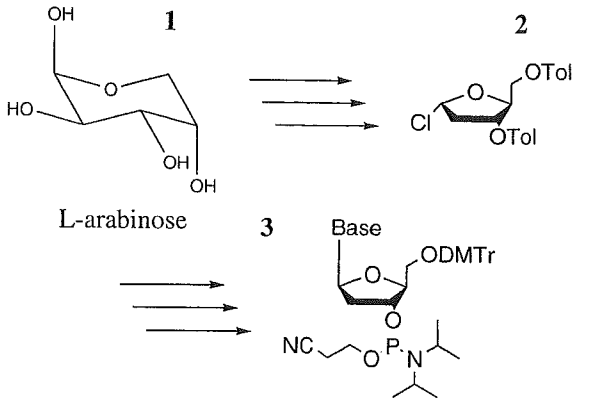

Scheme 1. Outline of synthesis scheme of L-deoxynucleoside phosphoramidite unit

d^{L}(GACAACGGAGACAGAGCAATTT)^{D}(CAATACGGGATAATACC) by a solid phase DNA synthesis method. This L-D chimera oligomer was purified by reverse phase HPLC and polyacrylamide gel electrophoresis (PAGE), and identified by MALDI-TOFMS. This oligomer consists of functionally two separated regions, D- and L-DNA; D-DNA region is served as primer for PCR and L-DNA region is served as a molecular tag. In the digestion experiment with the mixture of P1 nuclease and alkaline phosphatase, L-DNA region was little digested, although

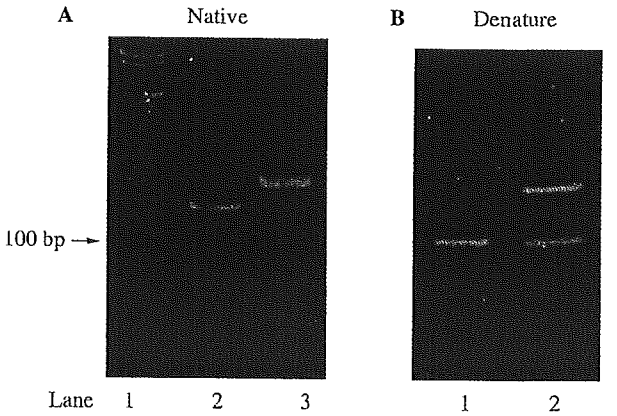

Figure 1. The results of PCR with L-D chimera primer. (**A**) 10 % native PAGE analysis of the PCR product; lane 1, DNA marker, lane 2, PCR product from normal primer consisting of only D-DNA, lane 3, PCR product from L-D chimera primer. (**B**) 8 % denaturing urea PAGE analysis of the PCR product; lane 1, PCR product from normal primer consisting of only D-DNA, lane 2, PCR product from L-D chimera primer

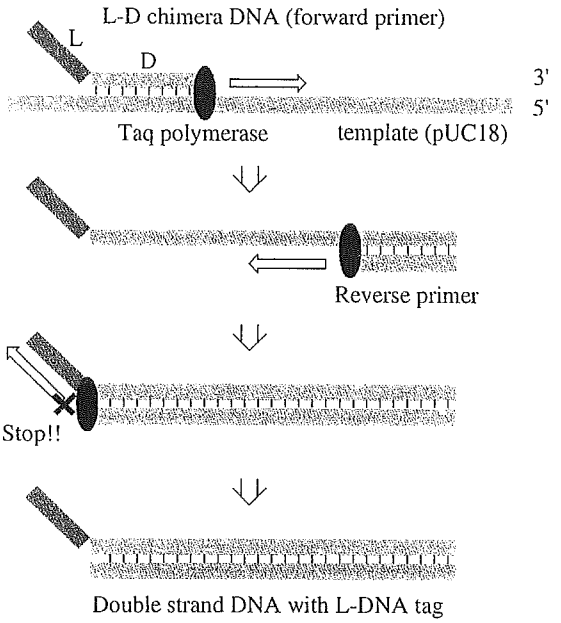

Figure 2. Schematic depiction of the polymerase extension reaction. Extension reaction starting from reverse primer stops at the boundary between L- and D-DNA region.

D-DNA region was completely digested to nucleotides. This result is consistent with L-DNA property.

With L-D chimera DNA in hand, the amplification reaction was carried out with 500 nM primers, Taq polymerase Master Mix (QIAGEN), 100 pg/μl template (puC18), for 35 cycles of 94°C x 30 sec, 55°C x 30 sec, 72°C x 1 min. The reaction mixture was analyzed by PAGE (Figure 1). A major product was observed in 140-150 bp region in lane 3, and its length is longer than normal PCR product, which was generated with normal forward primer from D-deoxyoligonucleotides, d^D(CAATACGGGATAATACC) (Figure 1A). In denaturing urea PAGE, two bands were clearly observed and the shorter band was the same length with normal PCR product (Figure 1B). This result suggested that in the process of PCR, L-DNA region could not be the PCR template and the polymerase extension reaction stopped at the boundary between L- and D-DNA region to obtain PCR product labelled by L-DNA (Figure 2). Further investigation using MALDI-TOFMS ensured that Taq polymerase could not elong even one nucleosides on L-DNA template.

The produced L-DNA tagged PCR products were exposed to SPR gold surface where L-DNA complementary with L-DNA tag were pre-immobilized. Two L-DNA having different sequence complementary with L-DNA tag part were immobilized on SPR gold chip through conventional method[6]. The address specific increase of SPR signal means that according to sequence information of L-DNA tagged PCR products, they hybridized to complementary L-DNA immobilized on SPR sensor chip. Thus, double strand DNA could be hybridized directly on the solid surface immobilizing L-DNA.

CONCLUSIONS

In these studies, usage of L-D chimera DNA as PCR primers leads to the formation of L-DNA tagged PCR products, which are very useful for immediate immobilization to the micro array. This novel method enables us to separate the multiple PCR products without any difficulties. This study is the first example for application of L-DNA to gene engineering.

ACKNOWLEDGEMENTS

We are grateful to the biotechnology group of TOYOBO Tsuruga Institute for excellent supports and advices.

REFERENCES

1. Williams, K. P., Liu, X., Schumacher, T. M., Lin, H., Ausiello, D. A., Kim, P. S. and Bartel, D. P. (1997) *Proc. Natl. Acad. Sci. USA*, **94**, 11285-11290.
2. Purschke, W. G., Radtke, F., Kleinjung, F. and Klussmann, S. (2003) *Nucleic Acid Res.*, **31**, 3027-3032.
3. Urata, H., Ogura, E., Shinohara, K., Ueda, Y. and Akagi, M. (1992) *Nucleic Acid Res.*, **20**, 3325-3332.
4. Shi, ZD., Yang, BH. and Wu YL. (2002) *Tetrahedron*, **50**, 3287-3296.
5. Hirschhorn, J. N., Skalr, P., Lindblad-Toh, K., Lim, Y., Ruiz-Gutierrez, M., Bolk, S., Langhorst, B., Schaffner, S., Winchester, E. and Landerm E. S. (2000) *Proc. Natl. Acad. Sci. USA*, **97**, 12164-12169
6. Kyo, M., Yamamoto, T., Motohashi, H., Kamiya, T., Kuroita, T., Tanaka, T., Engel, J. D., Kawakami, B. and Yamamoto, M. (2004) *Genes to Cells*, **9**, 153-164

Journal of Biomolecular NMR (2005) 31: 269–270
DOI 10.1007/s10858-005-0522-0

Letter to the Editor: ^{1}H, ^{15}N and ^{13}C backbone and side-chain assignments of the rice phytochrome B PAS1 domain and backbone assignments of the PAS1-PAS2 domain

Toshitatsu Kobayashi[a], Masaki Mishima[a], Kayo Akagi[b], Nobuya Sakai[b], Etsuko Katoh[b], Makoto Takano[b], Toshimasa Yamazaki[b] & Chojiro Kojima[a,*]

[a]*Graduate School of Biological Sciences, Nara Institute of Science and Technology (NAIST), 8916-5, Takayama, Ikoma, Nara, 630-0192, Japan;* [b]*2-1-2 Kan-non-dai, National Institute of Agrobiological Sciences, Tsukuba, 305-8602, Japan*

Received 08 November 2004; Accepted 23 December 2004

Key words: PAS, photomorphogenesis, phyB C-terminal, red/far-red light photoreceptor, rice

Biological context

Phytochromes consist of a family of red/far-red light photoreceptors in plants that regulate photomorphogenic events ranging from seed germination and deetiolation, to the induction of flowering (Neff et al., 2000). Following absorption of red light, phytochromes translocate from the cytoplasm to the nucleus, and subsequently regulate gene expression through interactions with transcription factors such as basic-helix-loop-helix proteins (Quail, 2002). Phytochrome proteins possess two major structural domains, the N- and C- terminal domains (Quail, 1997). The N-terminal domain (~74 kDa) possesses a covalently attached linear tetrapyrrole chromophore (phytochromobilin) and is sufficient for light absorption and photoreversibility. The C-terminal domain (~55 kDa), which plays a role in phytochrome dimerization and downstream signaling, consists of two PAS (PER-ARNT-SIM) domains and one histidine kinase-like domain. The PAS domains are a family of sensor protein domains involved in signal transduction in a wide range of organisms (Taylor and Zhulin, 1999). With phytochromes, a loss of function missense mutation cluster was located within the PAS domains, suggesting that these domains are crucial for phytochrome signaling (Quail et al., 1995; Ni et al., 1998; Chen et al., 2003; Matsushita et al., 2003). In an effort to delineate the mechanism underlying photomorphogenesis in plants, it is important to investigate the three- dimensional structure and dynamic aspects of this domain. The assignment of the rice phytochrome B PAS domains presented here represents the first step toward the study of phytochrome signaling using NMR.

*To whom correspondence should be addressed. E-mail: kojima@bs.naist.jp

Methods and experiments

The rice phytochrome B (phyB) PAS1 and PAS1-PAS2 domains (residues 666-782 and 666-923, respectively) were cloned into the pET32c expression vector (Novagen) and over-produced in *E. coli* BL21 (DE3) RIL (Novagen) as thioredoxin and hexa-histidine fusion proteins. $^{13}C/^{15}N$- or^{15}N-labeled protein was induced by the presence of 1 mM IPTG at 25 °C in M9 minimal medium containing $^{15}NH_4Cl$ and [U–^{13}C] glucose or unlabeled glucose, respectively. Cells obtained from M9 cultures were lysed by sonication. The lysate was centrifuged and the supernatant was loaded onto a Ni-NTA agarose resin (Qiagen). Proteins were eluted with imidazole in a stepwise manner. The sample fraction was then passed through a Superdex 26/60 75 pg gel filtration column (Amersham). Following removal of the fused tag by enterokinase (Novagen) was performed, Hi-trap Q anion-exchange (Amersham) and Superdex 26/60 75 pg columns were used to further purify the samples. The identity and integrity of the protein samples was confirmed by N-terminal sequencing, MALDI/TOF MS and SDS-PAGE.

All NMR measurements were carried out on a Bruker AV500 spectrometer equipped with a $^{1}H/^{13}C/^{15}N$ cryogenic probe and a DRX800 spectrometer

equipped with a $^{1}H/^{13}C/^{15}N/^{31}P$ probe at 30 °C. The PAS1 and PAS1-PAS2 domains were dissolved in 90%/10% H_2O/D_2O containing 50 mM phosphate (pH 6.8), 20 mM KCl and 5 mM DTT at a protein concentration of 0.8 mM and 0.2 mM, respectively. For the PAS1 domain, the backbone and side-chain resonances were obtained from the following spectra: HNCACB, HN(CO)CACB, HN(CA)CO, HNCO, C(CO)NH, H(CCO)NH, 4D-HC(CO)NH, HCCH-TOCSY, ^{15}N-edited TOCSY-HSQC and 2D-NOESY experiments. For the sequential backbone assignments of the PAS1-PAS2 domain, HNCACB, HN(CO)CACB, HN(CA)CO and HNCO were recorded. The NMR data were processed using NMRPipe (Delaglio et al., 1995) and analyzed using SPARKY (T. D. Goddard and D. G. Kneller, SPARKY 3, University of California, San Francisco).

Extent of assignments and data deposition

Supplementary Figure 1a and 1b show the $^{1}H/^{15}N$ HSQC spectra of the phyB PAS1 and phyB PAS1-PAS2 domains, respectively. The phyB PAS1 domain consists of 124 residues including 7 N-terminal residues originating from the vector, while the phyB PAS1-PAS2 domain consists of 261 residues including 3 residues from the vector. For the backbone atoms of the PAS1 domain, 97.5, 97.5, 97.5, 97.3 and 98.4% of the ^{1}HN, ^{15}N, $^{13}C_{\alpha}$, $^{13}C_{\beta}$ and $^{13}C'$ resonance assignments were obtained, respectively. For the aliphatic and aromatic side-chain atoms of the PAS1 domain, 92.7% of the ^{1}H and ^{13}C resonance assignments were obtained. For the PAS1-PAS2 domain, 98.4, 98.4, 98.9, 99.2 and 98.9% of the ^{1}HN, ^{15}N, $^{13}C_{\alpha}$, $^{13}C_{\beta}$ and $^{13}C'$ backbone resonance assignments were obtained. The L695-T696, L698, V709, I713-F714, K740-Q748 and K750-I756 in the PAS1 domain, and the V709, I713, T743-Q748, K750-G751 and V755 in the PAS1-PAS2 domain showed minor peaks. The chemical shift assignments (^{1}H, ^{15}N, ^{13}C) of the rice phyB PAS1 and PAS1-PAS2 domains have been deposited in the BioMagResBank (http://www.bmrb.wisc.edu) under accession number 6439 and 6440, respectively.

Acknowledgements

We thank Ryo Tabata for help in the early part of this work and Junko Tsukamoto for technical support in performing the N-terminal sequencing and MALDI/TOF MS analyses. This work was supported in part by Grants-in-Aid for Scientific Research and 21st Century COE Research from MEXT (the Ministry of Education, Culture, Sports, Science and Technology) of Japan, and a grant from the Ministry of Agriculture, Forestry and Fisheries of Japan (Rice Genome Project, PR-4101).

Supplementary material to this paper is available in electronic form at: http://dx.doi.org/10.1007/s10858-005-0522-0.

References

Chen, M., Schwab, R. and Chory, J. (2003) *Proc. Natl. Acad. Sci. USA.*, **24**, 14493–14498.
Delaglio, F., Grzesiek, S., Vuister, G.W., Zhu, G., Pfeifer, J. and Bax, A. (1995) *J. Biomol. NMR.*, **6**, 277–293.
Neff, M.M., Fankhauser, C. and Chory, J. (2000) *Genes Dev.*, **14**, 257–271.
Ni, M., Tepperman, J.M. and Quail, P.H. (1998) *Cell*, **95**, 657–667.
Matsushita, T., Mochizuki, N. and Nagatani, A. (2003) *Nature*, **424**, 571–574.
Quail, P.H., Boylan, M.T., Parks, B.M., Short, T.W., Xu, Y. and Wagner, D. (1995) *Science*, **268**, 675–680.
Quail, P.H. (1997) *Plant Cell Environ.*, **20**, 657–665.
Quail, P.H. (2002) *Nat. Rev. Mol. Cell Biol.*, **3**, 85–93.
Taylor, B.L. and Zhulin, B. (1999) *Microbiol. Mol. Biol. Rev.*, **63**, 479–506.

Biochemistry **2005,** *44,* 6144−6152

Linker Region of a Halobacterial Transducer Protein Interacts Directly with Its Sensor Retinal Protein†

Yuki Sudo,‡,§ Hideyasu Okuda,§ Masaki Yamabi,‡ Yuta Fukuzaki,§ Masaki Mishima,§ Naoki Kamo,‡ and Chojiro Kojima*,§

Laboratory of Biophysical Chemistry, Graduate School of Pharmaceutical Sciences, Hokkaido University, Sapporo 060-0812, Japan, and Laboratory of Biophysics, Graduate School of Biological Sciences, Nara Institute of Science and Technology, 8916-5 Takayama, Ikoma, Nara 630-0192, Japan

Received November 18, 2004; Revised Manuscript Received January 25, 2005

ABSTRACT: *p*HtrII, a *pharaonis* halobacterial transducer protein, possesses two transmembrane helices and forms a signaling complex with *pharaonis* phoborhodopsin (*p*pR, also called *pharaonis* sensory rhodopsin II, NpSRII) within the halobacterial membrane. This complex transmits a light signal to the sensory system located in the cytoplasm. It has been suggested that the linker region connecting the transmembrane region and the methylation region of *p*HtrII is important for binding to *p*pR and subsequent photosignal transduction. In this study, we present evidence to suggest that the linker region itself interacts directly with *p*pR in addition to the interaction in the membrane region. An *in vitro* pull-down assay revealed that the linker region bound to *p*pR, and its dissociation constant (K_D) was estimated to be approximately 10 μM using isothermal titration calorimetry (ITC). Solution NMR analyses showed that *p*pR interacted with the linker region of *p*HtrII (*p*HtrII$^{G83-Q149}$) and resulted in the broadening of many peaks, indicating structural changes within this region. These results suggest that the *p*HtrII linker region interacts directly with *p*pR. There was no demonstrable interaction between the C-terminal region of *p*pR (*p*pR$^{Gly224-His247}$) and either the linker region (*p*HtrII$^{G83-Q149}$) or the transmembrane region (*p*HtrII$^{M1-E114}$) of *p*HtrII. On the basis of the NMR, CD, and photochemical data, we discuss the structural changes and role of the linker region of *p*HtrII in relation to photosignal transduction.

The *pharaonis* halobacterial transducer protein, *p*HtrII, from *Natronomonas (Natronobacterium) pharaonis* (*1*), is a two-transmembrane helical protein and belongs to a family of two-transmembrane helical methyl-accepting chemotaxis proteins (MCPs) (*2*−*4*). MCPs exist as homodimers composed of a ~50−60-kDa subunit and form the ternary complex with CheA and CheW. Chemical stimuli activate phosphorylation cascades that modulate flagella motors (*5*). In relation to chemoreception in bacteria, MCPs act not only as transducers but also as signal receptors. In terms of photoreception in *Natronomonas pharaonis*, a direct interaction is required between *p*HtrII and the photosignal receptor *pharaonis* phoborhodopsin (*p*pR,[1] also called *pharaonis* sensory rhodopsin II, NpsRII) (*1*, *6*). *p*pR transmits light signals to *p*HtrII through changes resulting from the interaction, and *p*HtrII eventually activates phosphorylation cascades that modulate flagella motors. The active (signaling) intermediates of the *p*pR/*p*HtrII complex are referred to as the M and O intermediates (*7*). Using these sensing systems, *N. pharaonis* avoids harmful near-UV light (λ < 520 nm).

*p*pR is a member of the seven-transmembrane helical retinal group of proteins (*8*) that includes rhodopsin (*9*), bacteriorhodopsin (*10*), and others (*11*, *12*). *p*pR and *p*HtrII are stable within the membrane and *n*-dodecyl-β-D-maltoside micelles (*13*, *14*). Expression systems utilizing *Escherichia coli* cells can provide large amounts of *p*pR and *p*HtrII proteins (several mg/L culture) (*15*). Consequently, *p*pR and *p*HtrII have been well-characterized over the past few years using various methods (for reviews, see refs *1*, *8*, *16*, and *17*). Sudo et al. demonstrated a 2:2 stoichiometry in the *p*pR/*p*HtrII complex (*18*) and calculated the binding constant between *p*pR and *p*HtrII under various conditions (*19*, *20*). Figure 1 shows the crystal structure of the *p*pR/*p*HtrII complex (*21*). Of particular importance is the hydrogen-bonding network between Tyr199^{ppR} and Asn74^{pHtrII} and between Thr189^{ppR} and Glu43^{pHtrII}/Ser62^{pHtrII} and the phenolic ring of Tyr199^{ppR} and Phe28^{pHtrII} (*14*, *22*). Furthermore, the importance of Thr189^{ppR}, Asp193^{ppR}, and Thr204^{ppR} for the interaction has also been examined (Yamabi et al., manuscript in preparation).

*p*HtrII is composed of four regions consisting of two-transmembrane segments (TM1 and TM2), a linker region, a methylation region, and a signaling domain. Kim et al. reported on the X-ray structure of the methylation region and the signaling region of a serine chemotaxis receptor (Tsr)

† This work was supported by grants from Japanese Ministry of Education, Culture, Sports, Science, and Technology.

* To whom correspondence should be addressed. Telephone: 81-743-72-5571. Fax: 81-743-72-5579. E-mail: kojima@bs.naist.jp.

‡ Hokkaido University.

§ Nara Institute of Science and Technology.

[1] Abbreviations: *p*pR, *pharaonis* phoborhodopsin; *p*HtrII, *pharaonis* halobacterial transducer II; DM, *n*-dodecyl-β-D-maltoside; OG, *n*-octyl-β-D-glucoside; NMR, nuclear magnetic resonance; ITC, isothermal titration calorimetry; K_D, dissociation constant; GST, glutathione-*S*-transferase; CD, circular dichroism; HSQC, heteronuclear single-quantum correlation; TM, transmembrane segment; *p*HtrII$^{G83-Q149}$, *p*HtrII fragment from Gly83 to Gln149.

10.1021/bi047573z CCC: $30.25
Published on Web 03/26/2005

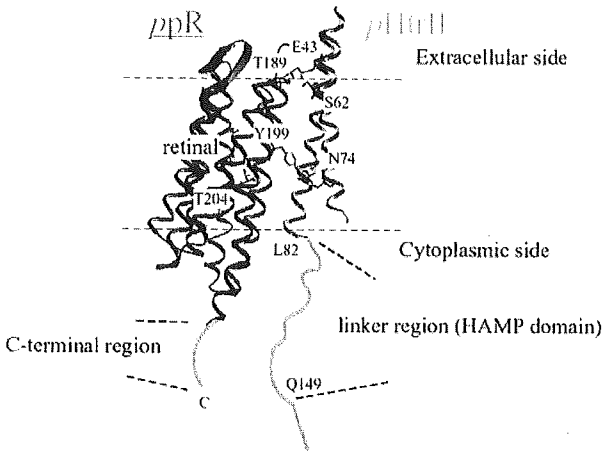

FIGURE 1: X-ray crystallographic structure of the *p*pR/*p*HtrII complex. The structure was obtained from the Protein Data Bank (PDB code 1H2S). *p*pR and *p*HtrII form the signaling complex in the dark and photolyzed state. Light stimulation activates *p*pR and triggers trans−cis photoisomerization of the retinal chromophore. Relaxation of the retinal leads to the functional processes during the photocycle. *p*pR transmits light signals to *p*HtrII in the membrane. *p*HtrII forms a ternary complex with CheA and CheW and activates phosphorylation cascades that modulate flagella motors. In this paper, the *p*HtrII linker region and the C-terminal region of *p*pR were designated as the regions from *p*HtrII^{Leu83} to *p*HtrII^{Gln149} and from *p*pR^{Gly224} to *p*pR^{His247}, respectively. The membrane normal is roughly in the vertical plane of this figure, and the top and bottom regions correspond to the extracellular and cytoplasmic sides, respectively.

(*23*). The X-ray structure of the transmembrane region of *p*HtrII in the *p*pR/*p*HtrII complex has recently been reported (*21*) (Figure 1). Tsr belongs to the two-transmembrane helical MCPs (*2*, *24*). Although these results have facilitated the next stage of research to do with photosignal transduction, detailed structural investigations concerning the linker region connecting the membrane region and the methylation region of MCPs have not been reported. The linker region posesses what is referred to as a HAMP domain, which is typically found in various proteins such as histidine kinases, adenylyl cyclases, methyl-accepting chemotaxis/phototaxis proteins, and phosphatases (*2*, *24*). This domain plays crucial roles in the phosphorylation or methylation of homodimeric receptors by transmitting conformational changes from the periplasmic to the cytoplasmic domain. It has been suggested that the linker region of the transducer may participate in the interaction with the sensor retinal pigment because certain residues within the linker region of HtrI (the *Halobacterium salinarum* transducer protein) modulate the sensory rhodopsin (sR, also called sensory rhodopsin I, sRI) photocycle (*4*, *25*). Umemura et al. reported that the sensing of cytoplasmic pH by chemoreceptors involves the linker region (*26*). Recently, Yang et al. reported that the E−F loop of *p*pR was located near the part of the *p*HtrII linker region based on probe accessibility data, disulfide formation assays, the flash photolysis analysis, as well as the FRET analysis (*27*). In this paper, we demonstrate that the linker region of *p*HtrII (*p*HtrII$^{G83-Q149}$) interacts directly with *p*pR.

MATERIALS AND METHODS

Protein Expression and Purification. The *p*pRHis (His refers to a hexa-histidine tag at the C terminus) expression plasmid was constructed as previously described (*28*). The GST-*p*HtrII$^{G83-Q149}$ gene was prepared by employing a PCR methodology. Primer 5′-GGATCCTGGGCGGTGACAC-CGCCGCCTCGCTTTC-3′ (the underlined bases indicate the added restriction site for *Bam*HI) and the reverse primer 5′-TTATGTGCCTGCTCTGCGTCCTCGCGAGCGTTC-3′ (the underlined bases indicate the added stop codon) were designed for the PCR. The PCR product was subcloned into the pGEM-T Easy (Promega) plasmid vector. The *Bam*HI and *Eco*RI digested fragment was ligated to a pGEX5X-3 vector (Amarsham). This cloning strategy resulted in the following N- and C-terminal peptide sequence: GST-*p*HtrII^{83}GGDTA- - -AEQAQ^{149}.

*p*pR was expressed in *E. coli* strain BL21 (DE3) (Invitrogen, Carlsbad, CA) at 37 °C in 2× YT medium containing ampicillin and subsequently induced by the addition of 1 mM IPTG and 10 μM all-*trans* retinal. Preparation of crude membranes and purification of *p*pR was performed as previously described (*29*). GST-*p*HtrII$^{G83-Q149}$ and GST only were overexpressed in *E. coli* strain BL21 (DE3) star cells (Invitrogen, Carlsbad, CA) and subsequently induced by the addition of 1 mM IPTG (Wako Pure Chemical Industries, Osaka, Japan). *p*pR proteins possessing a histidine tag at the C terminus were solubilized with 1.0% *n*-dodecyl-β-D-maltoside (DM) and subsequently purified using a Ni column as previously described (*29*).

IPTG-induced cells that expressed GST alone and GST-*p*HtrII linker were harvested by centrifugation at 4 °C. Pellets were resuspended in buffer A [50 mM Tris-HCl (pH 8.0) and 5 mM $MgCl_2$] and then broken by sonication. The supernatants were collected by ultracentrifugation (140000*g* for 30 min at 4 °C) to remove the membrane fraction. GST and GST-*p*HtrII$^{83-149}$ were then applied to a glutathione sepharose 4B resin column. The resin was washed extensively with buffer B [50 mM Tris-HCl (pH 8.0) and 300 mM NaCl] to remove nonspecifically bound proteins. GST and GST-tagged *p*HtrII were then eluted with buffer C [50 mM Tris-HCl (pH 8.0), 300 mM NaCl, and 10 mM glutathione]. The sample medium was exchanged by Amicon Ultra (Millipore, Bedford, MA) filtration and the samples were finally suspended in a buffer solution containing 150 mM NaCl, 50 mM Tris-HCl (pH 7.5), and 1 mM $CaCl_2$. Purified GST-*p*HtrII$^{83-149}$ was incubated with Factor Xa (0.5 unit/mg of protein) for ~3−4 h at 4 °C. The reaction was stopped by the addition of a protease inhibitor (1,5-dansyl-Glu-Gly-Arg-chloromethyl ketone dihydrochloride, Calbiochem). GST-digested *p*HtrII$^{G83-Q149}$ was separated by gel-filtration chromatography in a buffer solution containing 150 mM NaCl, 50 mM Tris-HCl (pH 7.5), and 1 mM $CaCl_2$. A final yield of 30 mg of *p*HtrII$^{83-149}$/L of cell culture was obtained.

Uniformly ^{15}N-single-labeled and ^{15}N-,^{13}C-double-labeled proteins for NMR experiments were prepared by growing the cells in standard minimal medium containing 0.5 g/L ^{15}N-ammonium chloride (Isotec Inc., Miamisburg, OH) or ^{15}N-ammonium chloride and 1.0 g/L ^{13}C-D-glucose (Isotec Inc., Miamisburg, OH). Transformed cells were initially grown at 37 °C in 1 mL of LB medium and were inoculated directly into 200 mL of isotope-labeled standard minimal M9 medium followed by inoculation in 4 L of labeled medium.

Binding Assay between the pHtrII Linker Region (pHtrII$^{G83-Q149}$) and ppR. GST-tagged *p*HtrII$^{G83-Q149}$, GST-digested *p*HtrII$^{G83-Q149}$, and *p*pR were concentrated by Amicon Ultra (Millipore, Bedford, MA) filtration. Buffer solutions were exchanged completely by dialysis against a buffer solution [300 mM NaCl, 10 mM Tris-HCl (pH 8.0), and 1% OG] for 1 week using a 3-kDa cutoff dialysis cassette (Molecular cut off, 3000, Daiichi Pure Chemicals Co. Ltd. Tokyo, Japan). The protein concentration of *p*pR and *p*HtrII was determined using the molar extinction coefficient at 500 nm (40 000 M^{-1} cm^{-1}) (*30*) and 280 nm (Tyr (1420 M^{-1} cm^{-1}), respectively.

An *in vitro* pull-down assay was performed using a glutathione sepharose column essentially as previously described (*18*, *31*). Purified *p*HtrII$^{G83-Q149}$ (300 μM) and *p*pR (30 μM) were mixed in a molar ratio of 1:10 in buffer B containing 1% OG and then incubated for 1 h at room temperature with gentle stirring. After the mixed samples were bound to the glutathione sepharose resin, the resin was poured into a chromatography column and washed extensively with buffer B (about 5-fold volume against the column volume) to remove nonspecifically bound proteins. Bound *p*pR was eluted with buffer C.

For the isothermal titration calorimetry (ITC) experiments, the *p*pR and *p*HtrII$^{G83-Q149}$ sample buffer solutions were exchanged completely by dialysis against a buffer solution [150 mM NaCl, 10 mM Tris-HCl (pH 8.0), and 0.05% DM] for 1 week using a 3-kDa cutoff dialysis cassette. The protein concentration of *p*pR and *p*HtrII was 0.35 and 0.03 mM, respectively. All ITC experiments were performed at 308 K on a VP-ITC Micro Calorimeter (Microcal Inc). For control experiments, DM-containing buffers were used to ensure that there was no effect because of the detergent. The binding parameters were estimated using the following binding scheme:

$$p\text{pR}/p\text{HtrII}_n \leftrightarrow p\text{pR} + np\text{HtrII}$$

where n represents the number of *p*HtrII molecules required for the formation of a complex with *p*pR. Data were evaluated by employing the Origin-ITC software package.

Flash Photolysis with or without pHtrII$^{G83-Q149}$. The apparatus and procedure for flash spectroscopy was essentially as previously described (*32*). The decay rate of the M photointermediate of the wild-type *p*pR (20 μM) with or without *p*HtrII$^{G83-Q149}$ (80 μM) and *p*HtrII$^{M1-L159}$ (80 μM) was observed at 350 nm. Truncated *p*HtrII expressed from position 1−159 was used instead of the whole protein because the truncated transducer tightly interacts with *p*pR [K_D = 0.1 μM (in the dark state)] (*22*). The temperature was maintained at 20 °C.

NMR Spectroscopy. NMR experiments for $^{13}C/^{15}N$-labeled *p*HtrII$^{G83-Q149}$ were performed at 283 K on a Bruker Avance 500 spectrometer with a ^{1}H [$^{13}C/^{15}N$] pulse field gradient cryogenic probe in a buffer solution containing 50 mM KCl and 50 mM KP_i (pH 6.5) without detergent. NMR experiments for $^{13}C/^{15}N$-labeled *p*pR were performed at 303 K on a Bruker Avance 500 spectrometer in a buffer solution containing 50 mM KCl, 10 mM citric acid (pH 5.0), and 3% 1,2-dihexanoyl-*sn*-glycero-3-phosphocholine (DHPC) as a detergent. The protein concentration was 1.8 and 0.4 mM for *p*HtrII and *p*pR, respectively. The assignments of the ^{1}H, ^{13}C, and ^{15}N resonances of *p*HtrII$^{G83-Q149}$ and *p*pR were obtained using ^{1}H-^{15}N HSQC and a series of triple-resonance experiments: HN(CO)CACB, HNCACB, HNCO, HN(CA)-CO, and (H)N(CO-TOCSY)NH incorporating pulsed field gradients, water flip-back pulses, and a sensitivity enhancement scheme. All data were processed using NMRPipe (*33*) and analyzed using Sparky (http://www.cgl.ucsf.edu/home/sparky/) (*34*). The NMR experiments for $^{13}C/^{15}N$-labeled *p*HtrII$^{G83-Q149}$ in the presence of *n*-octyl-β-D-glucoside (OG) were performed at 283 K on a Bruker Avance 500 MHz spectrometer in a buffer solution containg 50 mM KCl and 50 mM KP_i (pH 6.5).

CD Spectroscopy. The CD spectrum was recorded on a JASCO (Tokyo, Japan) J-720W CD spectropolarimeter. The CD spectrum was recorded between 260 and 200 nm (0.1 cm cell) at 0.1 nm intervals with a scan speed of 20 nm/min. Signals were averaged over 6 separate scans. The protein concentration was 20 μM in a buffer solution containing 50 mM KP_i, 50 mM KCl, and OG (free, 0.5, 1.0, and 7.2%).

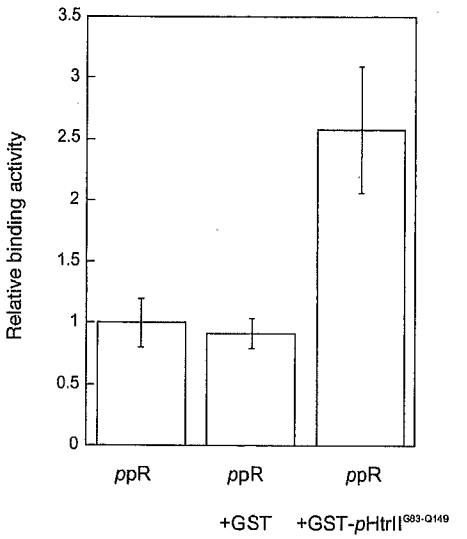

FIGURE 2: *In vitro* pull-down assay using glutathione sepharose resin. *p*pR was applied to the column without GST and GST-*p*HtrII$^{G83-Q149}$ (lane 1), with GST (lane 2), and with GST-*p*HtrII$^{G83-Q149}$ (lane 3). After the column was washed extensively with buffer B (for details, see the Materials and Methods) to remove nonspecifically bound proteins, bound proteins were eluted with buffer C (see the Materials and Methods). The eluted material was collected, and the UV−vis spectrum of *p*pR (λ_{max} = 500) was then measured.

RESULTS

Direct Interaction between the pHtrII Linker Region and ppR. In an effort to determine whether the *p*HtrII linker region (*p*HtrII$^{G83-Q149}$) interacts with *p*pR, we performed the *in vitro* pull-down assay (see the Materials and Methods and refs *18* and *31*). *p*pR adsorbed onto the glutathione sepharose 4B resin containing immobilized GST-*p*HtrII$^{G83-Q149}$. Figure 2 shows the adsorbed fraction of *p*pR in the presence of GST (lane 2) and in the absence or presence of GST-*p*HtrII$^{G83-Q149}$ (lanes 1 and 3, respectively). Specifically adsorbed *p*pR was detected in the presence of GST-*p*HtrII$^{G83-Q149}$.

The interaction between the *p*HtrII linker region (*p*HtrII$^{G83-Q149}$) and *p*pR was then quantitatively examined

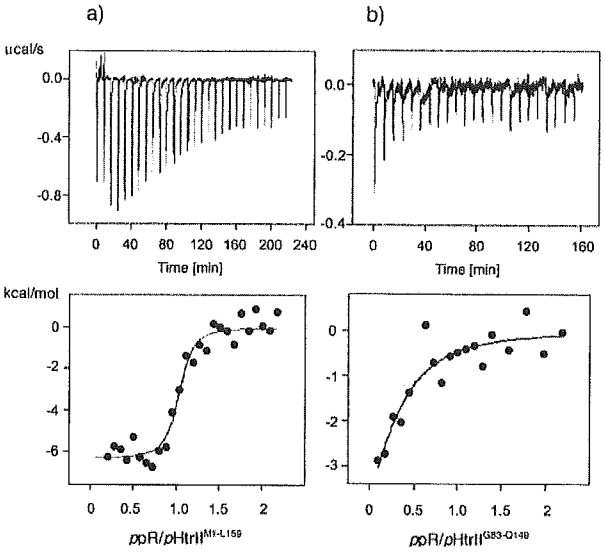

FIGURE 3: Isothermal calorimetric titration curves of *p*pR titrated with *p*HtrII$^{M1-L159}$ (a) and *p*HtrII$^{G83-Q149}$ (b). The upper panels represent the raw data. The lower panels represent the enthalpy changes per mole plotted as a function of the molar ratio of *p*pR to *p*HtrII. The solid lines represent best-fit curves (for details, see the Materials and Methods). The dilution heat of *p*pR is subtracted in these calculations. The binding parameters determined are listed in Table 1.

using ITC. Figure 3 shows the titration curves of *p*pR with *p*HtrII$^{M1-L159}$ and *p*HtrII$^{G83-Q149}$. Our ITC experiments were performed under the conditions established by Engelhard and co-workers (*22*). In these experiments, *p*HtrII$^{M1-L159}$ and *p*HtrII$^{G83-Q149}$ were maintained at 318 and 308 K, respectively, and *p*pR was added in increments of 10 μL using a syringe. The dissociation constant of *p*HtrII$^{M1-L159}$ (0.10 μM) was similar to the previously reported value (0.16 μM) (*22*). The dissociation constant (K_D) of *p*HtrII$^{G83-Q149}$ (10 μM) increased by nearly two orders and was almost identical to that of the signaling complex (*p*pR$_M$/*p*HtrII) (15 μM), as determined by flash photolysis (*18*). Our ITC results and those of other researchers are summarized in Table 1.

Table 1: Dissociation Constants (K_D) of Various *p*pR/*p*HtrII Mutant Complexes for the Ground State of *p*pR as Determined by ITC

	temperature (K)	pH	K_D (μM)	reference
*p*HtrII$^{M1-T157}$	318	8	0.16	*a*
*p*HtrII$^{M1-E114}$	318	8	0.23	*a*
*p*HtrII$^{M1-L159}$	318	8	0.1	this paper
*p*HtrII$^{G83-Q149}$	308	8	10	this paper
*p*HtrII$^{M1-L159}$ (interaction with *p*pR$_M$)	293	7.2	15	*b*

[a] Data from Hippler-Mreyen et al. (*22*). [b] Data from Sudo et al. (*18*).

From these binding assays, we concluded that the *p*HtrII linker region (*p*HtrII$^{G83-Q149}$) was able to interact directly with *p*pR in the dark state. Thus, the transmembrane and linker regions of *p*HtrII are both important in facilitating a direct and tight interaction with *p*pR.

Detailed Analysis of the Interaction between the pHtrII Linker Region and ppR by Solution NMR Spectroscopy. Solution NMR spectroscopy was performed in an effort to analyze the details of the *p*HtrII$^{G83-Q149}$–*p*pR interaction. Figure 4 shows a ^{1}H-^{15}N HSQC NMR spectrum of 1.8 mM *p*HtrII$^{G83-Q149}$ in 50 mM KP$_i$ (pH 6.5) and 50 mM KCl at

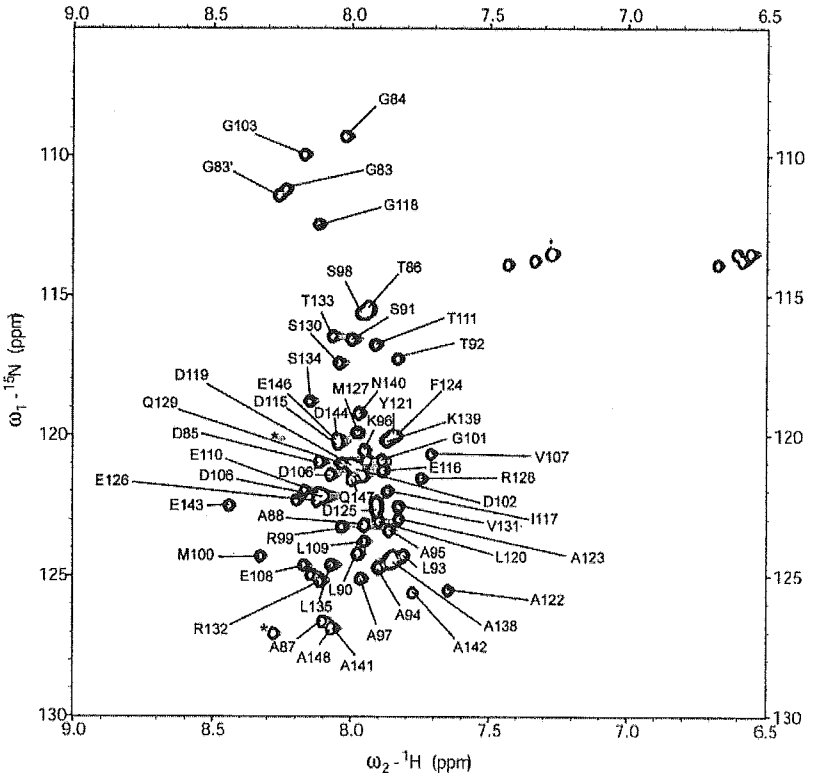

FIGURE 4: Two-dimensional ^{1}H-^{15}N HSQC spectrum of *p*HtrII$^{G83-Q149}$. The spectrum was recorded in 50 mM KCl and 50 mM KP$_i$ (pH 6.5) at 283 K on a 500 MHz NMR spectrometer. The assignments of the backbone amide protons are labeled.

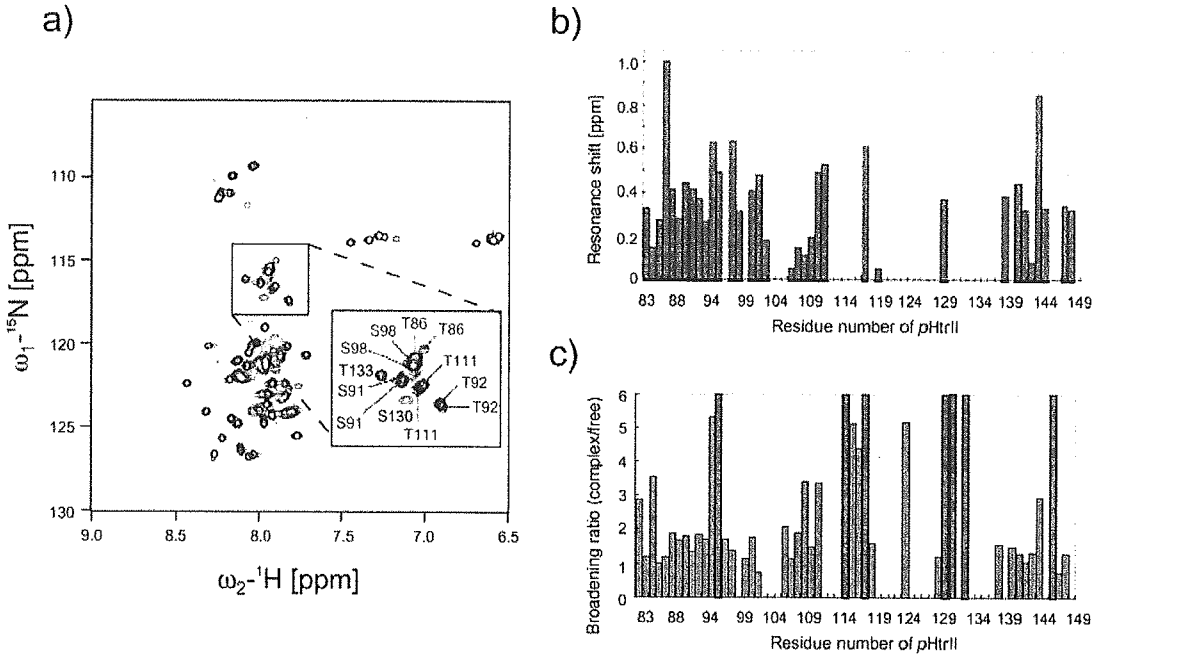

FIGURE 5: (a) Two-dimensional ^{1}H-^{15}N HSQC spectra of pHtrII$^{G83-Q149}$ with (blue) or without (red) ppR. Both spectra were recorded in 50 mM KP_i (pH 6.5) and 50 mM KCl at 283 K with 1% OG. (b and c) ppR-induced chemical-shift changes and the broadening ratios (complex/free ^{1}H line width), respectively, of the amide cross-peaks of pHtrII$^{G83-Q149}$.

283 K without detergent. Almost all of the signals from the backbone amide groups were observed. Backbone ^{1}H, ^{13}C, and ^{15}N resonances of 60 residues were assigned using conventional triple-resonance techniques, resulting in identification of the random structure based on ^{13}C chemical shifts. The assigned resonances are labeled in the figure. The ^{1}H-^{15}N HSQC spectra of 0.25 mM pHtrII$^{G83-Q149}$ in 50 mM KP_i (pH 6.5) and 50 mM KCl at 283 K with 1% OG as a detergent in the absence or presence of ppR (0.25 mM) are shown in Figure 5a as red and blue, respectively. ppR-induced resonance shifts and broadening were detected for many peakes, indicating that pHtrII$^{G83-Q149}$ interacts with ppR. This result is consistent with results of the aforementioned binding assays (Figures 2 and 3). Parts b and c of Figure 5 show the amino acid residues of pHtrII$^{G83-Q149}$ that showed resonance shifts and broadening, respectively, induced following association with ppR. The broadening of the resonance peaks originated from the middle part of the linker region (pHtrII$^{E114-R132}$), indicating that some structural changes in this region may occur.

Effect of the C-Terminal Region of ppR on the Interaction with the pHtrII Linker Region. The interaction between ppR and the pHtrII linker region (pHtrII$^{G83-Q149}$) was examined using stable isotope-labeled ppR (not pHtrII). Figure 6a shows a ^{1}H-^{15}N two-dimensional NMR spectrum of 0.4 mM ppR in 10 mM citric acid (pH 5.0) and 50 mM KCl at 303 K. Backbone ^{1}H, ^{13}C, and ^{15}N resonances of 23 residues in the C-terminal region of ppR (Figure 6b) were assigned using a conventional triple-resonance procedure. The assigned resonances are labeled in the figure. The ^{1}H-^{15}N HSQC spectra of 0.20 and 0.3 mM ppR in the absence or presence of 0.20 mM pHtrII$^{G83-Q149}$ and 0.3 mM of pHtrII$^{M1-E114}$ are shown in parts d and c of Figure 6, respectively. pHtrII-induced resonance shifts and broadening were not detected. Thus, the C-terminal region of ppR (ppR$^{Gly224-His247}$) does not participate in the interaction with pHtrII within the detergent micelles.

Does pHtrII Linker Region Interact with the M Photointermediate of ppR? Sudo et al. estimated the K_D value of the complex between the M intermediate of ppR (ppR$_M$) and pHtrII$^{M1-L159}$ (*18*). In an effort to determine whether this linker region (pHtrII$^{G83-Q149}$) can interact with ppR$_M$, a photochemical assay (see the Materials and Methods and refs *19* and *20*) was employed. Figure 7 shows the decay of the M photointermediate of ppR in the presence or absence of pHtrII. The decays of ppR$_M$ with or without pHtrII$^{M1-L159}$ are shown as gray lines, reproduced from ref *18*, and that of ppR$_M$ with pHtrII$^{G83-Q149}$ is shown as black dots. The molecular ratios of both ppR/pHtrII$^{M1-L159}$ and pHtrII$^{G83-Q149}$ were 1:10. The decay rate constant of the M photointermediate of ppR in the absence or presence of pHtrII$^{M1-L159}$, as well as that in the presence of pHtrII$^{G83-Q149}$, was 1.66, 0.82, and 1.69 s^{-1}, respectively. No significant change in the M decay rate was observed when pHtrII$^{83-149}$ was added to a molar ratio of ppR/pHtrII$^{G83-Q149}$ = 1:30 (data not shown). When ppR interacts with pHtrII$^{M1-L159}$, the decay rate of the M photointermediate of ppR changes ~2−4-fold. Thus, pHtrII$^{G83-Q149}$ does not interact with ppR$_M$, although the fragment might still physically interact but possibly not sufficiently to alter the decay rate.

DISCUSSION

Hippler-Mreyen et al. reported that the dissociation constant of pHtrII$^{M1-T157}$ (0.16 μM) was nearly 3 orders smaller than the value of pHtrII^{M1-L82} (>100 μM) (*22*). pHtrII^{M1-L82} lacks the linker region of pHtrII. They concluded that pHtrII$^{G83-T157}$ is important for the interaction with ppR. Yang et al. made use of the fluorescence resonance energy

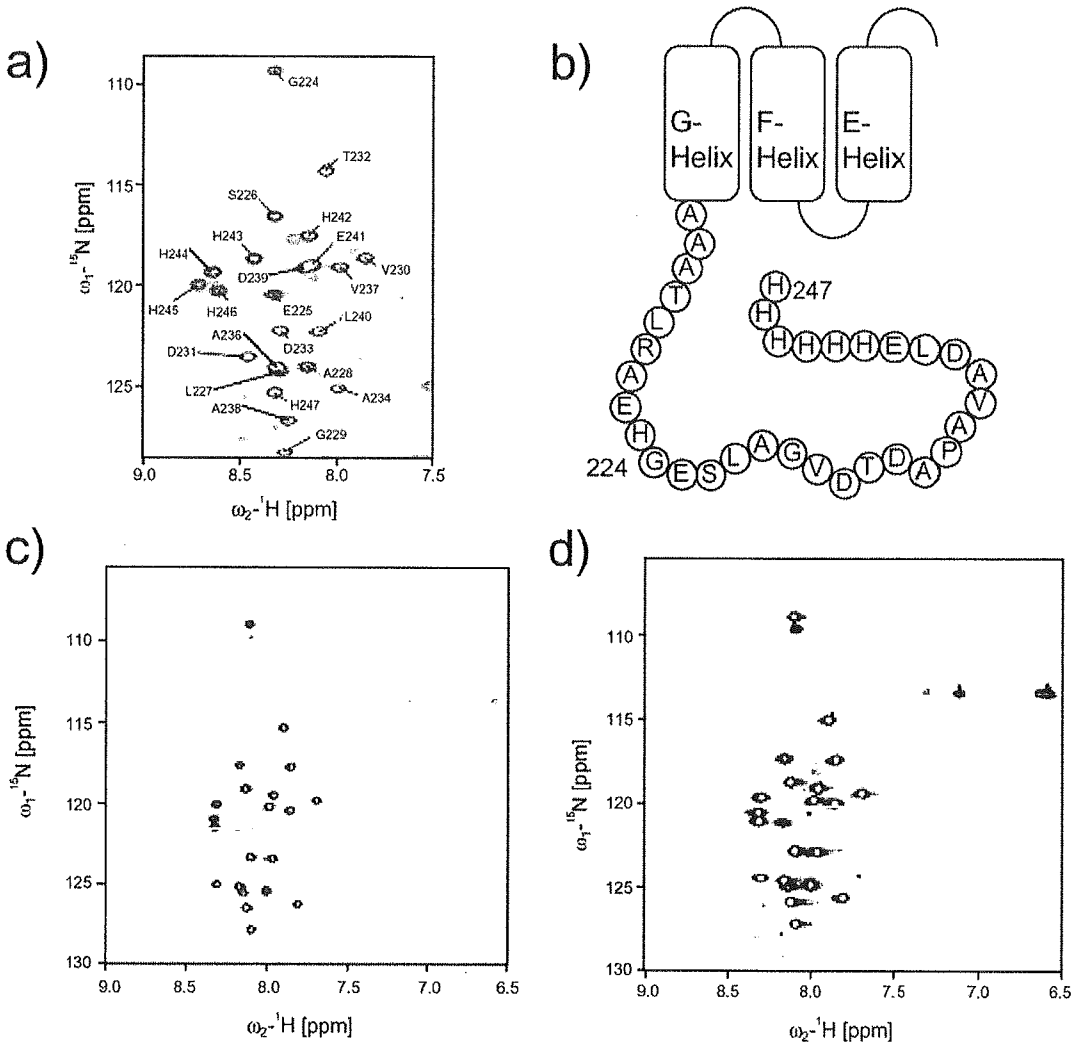

FIGURE 6: (a) Two-dimensional ^{1}H-^{15}N HSQC spectrum of *p*pR. The spectrum was recorded in 50 mM KCl and 50 mM KP_i (pH 6.5) at 283 K on a 500 MHz NMR spectrometer. The assignments of the backbone amide protons are labeled. (b) 23 residues located in the C-terminal region of *p*pR that were assigned. (c and d) ^{1}H-^{15}N HSQC spectra of the ^{15}N-labeled *p*pR in the absence (red) or presence (blue) of *p*HtrII$^{G83-Q149}$ (c) and *p*HtrII$^{M1-E114}$ (d).

transfer (FRET) method and concluded that the interaction site of *p*pR with the linker region is located near Ser-154 (*27*). From mutation analyses, Spudich and co-workers reported that *p*HtrII^{Gly83} and *p*HtrII^{Ala88} are important residues involved in photosignal transduction (*35*). In this paper, we demonstrated that the *p*HtrII linker region interacted directly with *p*pR. Our results are consistent with their data. Thus, the *p*HtrII linker region is important in facilitating a direct interaction with *p*pR that eventually results in phototransduction by the *p*pR/*p*HtrII complex.

OG was used as a detergent in the solution NMR analyses because *p*pR was not stable in the detergent-free solution. However, OG may affect the structure of the *p*HtrII linker region. From the CD spectroscopic measurements, it was determined that the secondary structure of the linker region changed from a random to an α-helical structure following the addition of OG. The cmc of the detergent (about 1%) is critical in determining the formation of the α helix (Figure 8a). This result is consistent with NMR experiments where the addition of OG altered the ^{1}H-^{15}N HSQC spectra in a manner dependent on the micelle concentration of OG (Figure 8b). Additionally, the resonance shifts and broadening were mainly detected in two short regions, the N-terminal and C-terminal parts of the *p*HtrII linker region, suggesting the formation of two α helices. These results suggest that the linker region would act as the chameleon sequence. Formation of an α helix is consistent with the data presented by Danielson et al., where the linker region of Tar corresponding to the *p*HtrII linker region forms an α helix by the cysteine and disulfide bond scanning method (*36*).

The nature of the OG-induced resonance shifts and broadening related to the *p*HtrII linker region was clearly different from those of the *p*pR-induced spectral changes (see Figures 5 and 8). These results reflect the presence of a specific interaction between the *p*HtrII linker region and *p*pR and that the observations made were not derived from detergent-induced changes. *p*pR-induced chemical-shift changes of the *p*HtrII signals mainly occurred in the N-terminal part of the *p*HtrII linker region spanning about 20 residues, suggesting that this N-terminal region possesses specific binding sites for *p*pR.

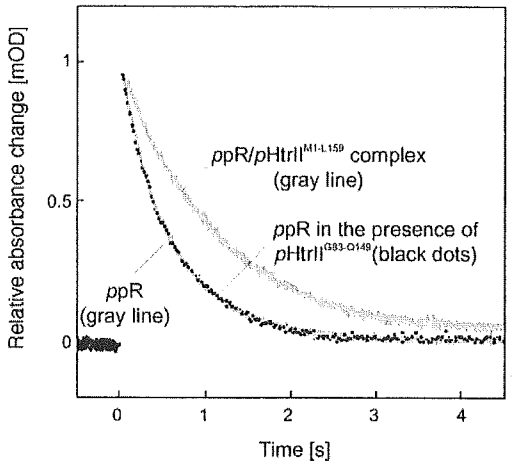

FIGURE 7: Decay of the M photointermeditate of *pp*R with or without *ph*HtrII$^{G83-Q149}$ and *ph*HtrII$^{M1-L159}$. The decay was monitored at 350 nm. Samples were suspended in a buffer solution containing 400 mM NaCl, 10 mM Tris-HCl (pH 7.0), and 1% *n*-dodecyl-*β*-D-maltoside (DM). The temperature was maintained at 20 °C. The decay curves of ppR_M with or without *ph*HtrII$^{M1-L159}$ are represented by gray lines, and that with *ph*HtrII$^{G83-Q149}$ is represented by black dots.

From the flash photolysis analysis, it was concluded that *ph*HtrII$^{G83-Q149}$ does not interact with ppR_M (Figure 7). Signal transduction from *pp*R to *ph*HtrII is accompanied by a weakened interaction with ppR_M (*14*, *18*, *22*, *31*). Therefore, it seems that the *ph*HtrII linker region is perturbed by the M state of *pp*R; that is, the interaction between *pp*R and *ph*HtrII becomes weak. Wegener et al. reported that the F helix of *pp*R moves toward *ph*HtrII following light activation of *pp*R (*37*). Helix movement during the photocycle in bacteriorhodopsin (BR) has also been reported (*38*, *39*). The helix movement of *pp*R is the signaling trigger to *ph*HtrII. Engelhard and co-workers reported that the TM-2 of *ph*HtrII rotates by following helix movement of *pp*R (*40*) and have suggested that the switch is in the M1 to M2 reaction (*41*). On the basis of the evidence given in this paper, a new photosignal transduction model is proposed (Figure 9). The movement of the helix in *pp*R and rotation of the TM-2 helix in *ph*HtrII occurs. Dissociation and conformational changes in the *ph*HtrII linker region, as demonstrated in this paper, follows. Thus, the association/dissociation of the *ph*HtrII linker region acts as a signaling switch in this model. Our model is consistent with the paper by Yang et al. (*27*) that the G83F mutant of *ph*HtrII, which eliminates the interaction with *pp*R, also eliminates phototaxis signaling.

In conclusion, we show that the *ph*HtrII linker region (*ph*HtrII$^{G83-Q149}$) interacts directly with *pp*R. Solution NMR analyses in the presence or absence of *pp*R showed that the global structural change of the *ph*HtrII linker region occurs because of association with *pp*R. The CD and NMR measurements at various OG concentrations revealed that the *ph*HtrII$^{G83-Q149}$ conformational changes are caused by a direct and specific interaction with *pp*R. Flash photolysis analysis showed that *ph*HtrII$^{G83-Q149}$ could not interact with *pp*R at the M state. Because the signal transduction from *pp*R to *ph*HtrII is accompanied by a weakened interaction with ppR_M, the dissociation and subsequent conformational changes of the *ph*HtrII linker region that follow can effect a transfer of the signal downstream. We propose this scheme as the "linker switch model" for photosignal transduction.

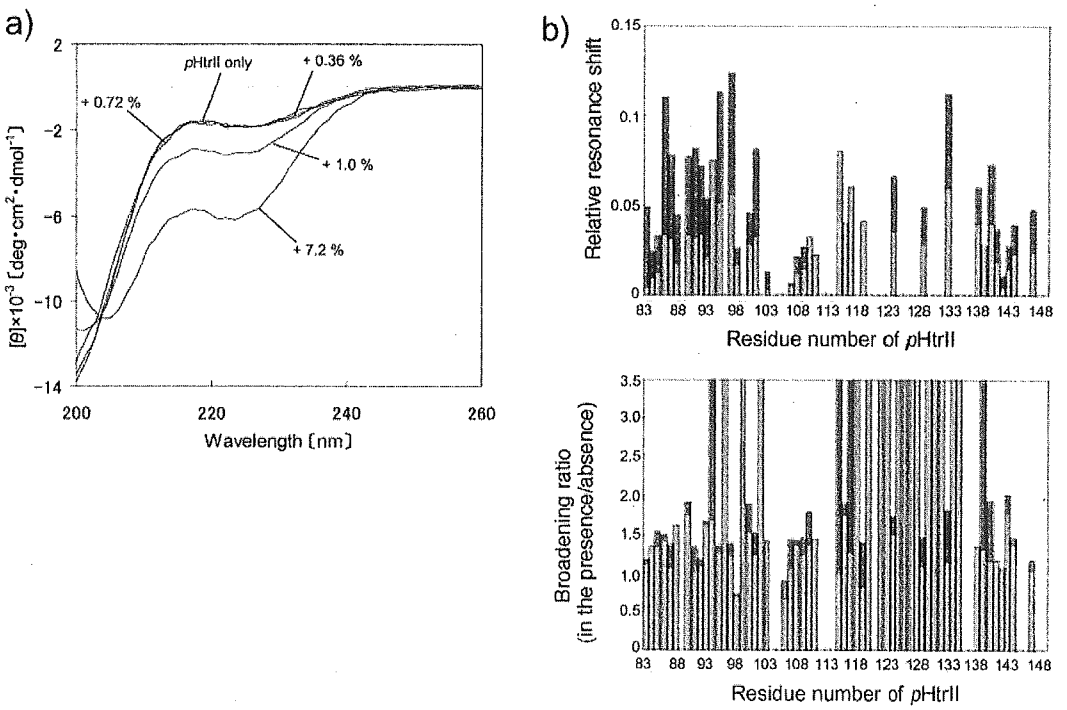

FIGURE 8: (a) CD spectrum of *ph*HtrII$^{G83-Q149}$ at various concentrations of OG detergent. The CD spectrum was recorded on a JASCO J-720W CD spectropolarimeter between 200 and 260 nm at 283 K. The spectrum obtained was baseline-corrected. (b) OG-induced chemical-shift changes (top) and the broadening ratios (bottom) (^{1}H line width in the presence/absence of OG) of the ^{1}H-^{15}N HSQC cross-peaks of *ph*HtrII$^{G83-Q149}$. Gray bars and black bars in b show the OG-induced changes in the presence of 1.0 and 7.2% OG, respectively.

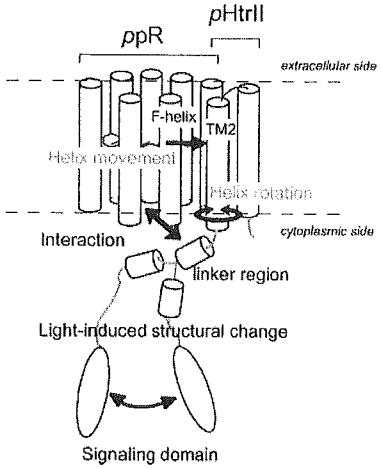

FIGURE 9: Model for photosignal transduction. The photoinduced conformational changes of *p*pR are transmitted to *p*HtrII. Rotation of the F helix of *p*pR induces structural changes in *p*HtrII. Simultaneous dissociation and conformational changes in the linker region then follow. The signal can subsequently be transmitted to CheW and CheA that form a ternary complex with *p*HtrII. Thus, the *p*HtrII linker region can be thought of as a molecular switch for signal transduction.

ACKNOWLEDGMENT

We thank Dr. Harumi Fukada for expert technical assistance in ITC measurement and critical reading of the manuscript and Junko Tsukamoto in N-terminal sequencing and TOF mass spectroscopy. We also thank Toshitatsu Kobayashi for valuable discussions.

REFERENCES

1. Sudo, Y., Kandori, H., and Kamo, N. (2004) Molecular mechanism of protein−protein interaction of *pharaonis* phoborhodopsin/transducer and photosignal transfer reaction by the complex, *Recent Res. Dev. Biophys. 3*, 1−16.
2. Rudolph, J., Nordmann, B., Storch, K. F., Gruenberg, H., Rodewald, K., and Oesterhelt, D. (1996) A family of halobacterial transducer proteins, *FEMS Microbiol. Lett. 139*, 161−168.
3. Falke, J. J., Bass, R. B., Butler, S. L., Chervitz, S. A., and Danielson, M. A. (1997) The two-component signaling pathway of bacterial chemotaxis: A molecular view of signal transduction by receptors, kinases, and adaptation enzymes, *Annu. Rev. Cell Dev. Biol. 13*, 457−512.
4. Hoff, W. D., Jung, K. H., and Spudich, J. L. (1997) Molecular mechanism of photosignaling by archaeal sensory rhodopsins, *Annu. Rev. Biophys. Biomol. Struct. 26*, 223−258.
5. Falke, J. J., and Hazelbauer, G. L. (2001) Transmembrane signaling in bacterial chemoreceptors, *Trends Biochem. Sci. 26*, 257−265.
6. Zhang, X. N., Zhu, J., and Spudich, J. L. (1999) The specificity of interaction of archaeal transducers with their cognate sensory rhodopsins is determined by their transmembrane helices, *Proc. Natl. Acad. Sci. U.S.A. 96*, 857−862.
7. Yan, B., Takahashi, T., Johnson, R., and Spudich, J. L. (1991) Identification of signaling states of a sensory receptor by modulation of lifetimes of stimulus-induced conformations: The case of sensory rhodopsin II, *Biochemistry 30*, 10686−10692.
8. Iwamoto, M., Kandori, H., and Kamo N. (2003) Photochemical properties of *pharaonis* phoborhodopsin (sensory rhodopsin II), *Recent Res. Devel. Chem. 1*, 15−30.
9. Hubbell, W. L., Altenbach, C., Hubbell, C. M., and Khorana, H. G. (2003) Rhodopsin structure, dynamics, and activation: A perspective from crystallography, site-directed spin labeling, sulfhydryl reactivity, and disulfide cross-linking, *Adv. Protein Chem.* 243−290.
10. Lanyi, J. K., and Luecke, H. (2001) Bacteriorhodopsin, *Curr. Opin. Struct. Biol. 11*, 415−419.
11. Bieszke, J. A., Braun, E. L., Bean, L. E., Kang, S., Natvig, D. O., and Borkovich, K. A. (1999) The nop-1 gene of neurospora crassa encodes a seven transmembrane helix retinal-binding protein homologous to archaeal rhodopsins, *Proc. Natl. Acad. Sci. U.S.A. 96*, 8034−8039.
12. Beja, O., Aravind, L., Koonin, E. V., Suzuki, M. T., Hadd, A., Nguyen, L. P., Jovanovich, S. B., Gates, C. M., Feldman, R. A., Spudich, J. L., Spudich, E. N., and DeLong, E. F. (2000) Bacterial rhodopsin: Evidence for a new type of phototrophy in the sea, *Science 289*, 1902−1906.
13. Ikeura, Y., Shimono, K., Iwamoto, M., Sudo, Y., and Kamo, N. (2003) Arg-72 of *pharaonis* phoborhodopsin (sensory rhodopsin II) is important for the maintenance of the protein structure in the solubilized state, *Photochem. Photobiol. 77*, 96−100.
14. Sudo, Y., Yamabi, M., Iwamoto, M., Shimono, K., and Kamo, N. (2003) Interaction of *Natronobacterium pharaonis* phoborhodopsin (sensory rhodopsin II) with its cognate transducer probed by increase in the thermal stability, *Photochem. Photobiol. 78*, 511−516.
15. Shimono, K., Iwamoto, M., Sumi, M., and Kamo, N. (1997) Functional expression of *pharaonis* phoborhodopsin in *Escherichia coli*, *FEBS Lett. 420*, 54−56.
16. Spudich, J. L. (2002) Spotlight on receptor/transducer interaction, *Nat. Struct. Biol. 9*, 797−799.
17. Klare, J. P., Gordeliy, V. I., Labahn, J., Büldt, G., Steinhoff, H. J., and Engelhard, M. (2004) The archaeal sensory rhodopsin II/transducer complex: A model for transmembrane signal transfer, *FEBS Lett. 564*, 219−224.
18. Sudo, Y., Iwamoto, M., Shimono, K., and Kamo, N. (2001) *pharaonis* phoborhodopsin binds to its cognate truncated transducer even in the presence of a detergent with a 1:1 stoichiometry, *Photochem. Photobiol. 74*, 489−494.
19. Sudo, Y., Iwamoto, M., Shimono, K., and Kamo, N. (2002) Tyr-199 and charged residues of *pharaonis* phoborhodopsin are important for the interaction with its transducer, *Biophys. J. 83*, 427−432.
20. Sudo, Y., Iwamoto, M., Shimono, K., and Kamo, N. (2004). Role of charged residues of *pharaonis* phoborhodopsin (seonsory rhodopsin II) in its interaction with the transducer protein, *Biochemistry 43*, 13748−13754.
21. Gordeliy, V. I., Labahn, J., Moukhametzianov, R., Efremov, R., Granzin, J., Schlesinger, R., Buldt, G., Savopol, T., Scheidig, A. J., Klare, J. P., and Engelhard, M. (2002) Molecular basis of transmembrane signalling by sensory rhodopsin II−transducer complex, *Nature 419*, 484−487.
22. Hippler-Mreyen, S., Klare, J. P., Wegener, A. A., Seidel, R., Herrmann, C., Schmies, G., Nagel, G., Bamberg, E., and Engelhard, M. (2003) Probing the sensory rhodopsin II binding domain of its cognate transducer by calorimetry and electrophysiology, *J. Mol. Biol. 330*, 1203−1213.
23. Kim, K. K., Yokota, H., and Kim, S. H. (1999) Four-helical-bundle structure of the cytoplasmic domain of a serine chemotaxis receptor, *Nature 400*, 787−792.
24. Aravind, L., and Ponting, C. P. (1999) The cytoplasmic helical linker domain of receptor histidine kinase and methyl-accepting proteins is common to many prokaryotic signalling proteins, *FEMS Microbiol. Lett. 176*, 111−116.
25. Jung, K. H., and Spudich, J. L. (1996) Protonatable residues at the cytoplasmic end of transmembrane helix-2 in the signal transducer HtrI control photochemistry and function of sensory rhodopsin I, *Proc. Natl. Acad. Sci. U.S.A. 93*, 6557−6561.
26. Umemura, T., Matsumoto, Y., Ohnishi, K., Homma, M., and Kawagishi, I. (2002) Sensing of cytoplasmic pH by bacterial chemoreceptors involves the linker region that connects the membrane-spanning and the signal- modulating helices, *J. Biol. Chem. 277*, 1593−1598.
27. Yang, C. S., Sineshchekov, O., Spudich, E. N., and Spudich, J. L. (2004) The cytoplasmic membrane-proximal domain of the HtrII transducer interacts with E−F loop of photoactivated *Nactronomonas pharaonis* sensory rhodopsin II, *J. Biol. Chem. 279*, 42964−42969
28. Sudo, Y., Furutani, Y., Shimono, K., Kamo, N., and Kandori, H. (2003) Hydrogen bonding alteration of Thr-204 in the complex between *pharaonis* phoborhodopsin and its transducer protein, *Biochemistry 42*, 14166−14172.
29. Kandori, H., Shimono, K., Sudo, Y., Iwamoto, M., Shichida, Y., and Kamo, N. (2001) Structural changes of *pharaonis* phoborhodopsin upon photoisomerization of the retinal chromophore: Infrared spectral comparison with bacteriorhodopsin, *Biochemistry 40*, 9238−9246.

30. Chizhov, I., Schmies, G., Seidel, R., Sydor, J. R., Luttenberg, B., and Engelhard, M. (1998) The photophobic receptor from *Natronobacterium pharaonis*: Temperature and pH dependencies of the photocycle of sensory rhodopsin II, *Biophys. J. 75*, 999−1009.
31. Sudo, Y., Iwamoto, M., Shimono, K., and Kamo, N. (2002) Association between a photointermediate of a M-lacking mutant D75N of *pharaonis* phoborhodopsin and its cognate transducer, *J. Photochem. Photobiol., B 67*, 171−176.
32. Miyazaki, M., Hirayama, J., Hayakawa, M., and Kamo, N. (1992) Flash photolysis study on *pharaonis* phoborhodopsin from a haloalkaliphilic bacterium (*Natronobacterium pharonis*), *Biochim. Biophys. Acta 1140*, 22−29.
33. Delaglio, F., Grzesiek, S., Vuister, G. W., Zhu, G., Pfeifer, J., and Bax, A. (1995) NMRPipe: A multidimensional spectral processing system based on UNIX pipes, *J. Biomol. NMR 6*, 277−293.
34. Goddard, T. D., and Kneller, D. G. *SPARKY 3*, University of California, San Francisco, CA.
35. Yang, C. S., and Spudich, J. L. (2001) Light-induced structural changes occur in the transmembrane helices of the *Natronobacterium pharaonis* HtrII transducer, *Biochemistry 40*, 14207−14214.
36. Danielson, M. A., Bass, R. B., and Falke, J. J. (1997) Cysteine and disulfide scanning reveals a regulatory α-helix in the cytoplasmic domain of the aspartate receptor, *J. Biol. Chem. 272*, 32878−32888.
37. Wegener, A. A., Chizhov, I., Engelhard, M., and Steinhoff, H. J. (2000) Time-resolved detection of transient movement of helix F in spin-labeled *pharaonis* sensory rhodopsin II, *J. Mol. Biol. 301*, 881−891.
38. Vonck, J. (2000) Structure of the bacteriorhodopsin mutant F219L N intermediate revealed by electron crystallography, *EMBO J. 19*, 2152−2160.
39. Radzwill, N., Gerwert, K., and Steinhoff, H. J. (2001) Time-resolved detection of transient movement of helices F and G in doubly spin-labeled bacteriorhodopsin, *Biophys. J. 80*, 2856−2866.
40. Wegener, A. A., Klare, J. P., Engelhard, M., and Steinhoff, H. J. (2001) Structural insights into the early steps of receptor-transducer signal transfer in archaeal phototaxis, *EMBO J. 20*, 5312−5319.
41. Rivas, L., Hippler-Mreyen, S., Engelhard, M., and Hildebrandt, P. (2003) Electric-field dependent decays of two spectroscopically different M-states of photosensory rhodopsin II from *Natronobacterium pharaonis*, *Biophys. J. 84*, 3864−3873.

BI047573Z

Solution Structure of the Peptidoglycan Binding Domain of *Bacillus subtilis* Cell Wall Lytic Enzyme CwlC: Characterization of the Sporulation-Related Repeats by NMR[†,‡]

Masaki Mishima,[§] Toshio Shida,[∥] Kazuto Yabuki,[§] Ken-ichi Kato,[§] Junichi Sekiguchi,[∥] and Chojiro Kojima*[,§]

Graduate School of Biological Sciences, Nara Institute of Science and Technology, 8916-5 Takayama, Ikoma 630-0101, Japan, and Department of Applied Biology, Faculty of Textile Science and Technology, Shinshu University, Tokida, Japan

Received April 5, 2005; Revised Manuscript Received May 29, 2005

ABSTRACT: *Bacillus subtilis* CwlC is a cell wall lytic *N*-acetylmuramoyl-L-alanine amidase that plays an important role in mother-cell lysis during sporulation. The enzyme consists of an N-terminal catalytic domain with C-terminal tandem repeats. The repeats [repeat 1 (residues 184−219) and repeat 2 (residues 220−255)] are termed CwlCr. We report on the solution structure of CwlCr as determined by multidimensional NMR, including the use of 36 $^{h3}J_{NC'}$-derived hydrogen bond restraints and 64 residual $^{1}D_{NH}$ dipolar couplings. Two tandem repeats fold into a pseudo-2-fold symmetric single-domain structure consisting of a $\beta\alpha\beta\beta\alpha\beta$-fold containing numerous contacts between the repeats. Hydrophobic residues important for structural integrity are conserved between the repeats, and are located symmetrically. We also present NMR analysis of the circularly permuted repeat mutant of CwlCr. Secondary structure content from the chemical shifts and hydrogen bonds derived from $^{h3}J_{NC'}$ show that the mutant folds into a structure similar to that of the wild type, suggesting that the repeats are exchangeable. This implies that conserved hydrophobic residues are crucial for maintaining the folding of the repeats. While monitoring the chemical shift perturbations following the addition of digested soluble peptidoglycan fragments, we identified two peptidoglycan interaction sites of CwlCr at the edges of the protein symmetrically, and they are located ~28 Å from each other.

Bacillus subtilis utilizes a set of enzymes capable of hydrolyzing the peptidoglycan layer of its own cell wall (*1*−*3*). Some of these peptidoglycan hydrolases can trigger cell lysis and are termed autolysins (*1*). These have been implicated in several important cellular processes, including cell wall turnover, cell separation, competence, and motility (*1*, *4*, *5*). *N*-Acetylmuramoyl-L-alanine amidases, which constitute the major autolysins, cleave the amido bond between the lactyl group of an *N*-acetylmuramic acid residue and the α-amino group of an alanine residue (*6*). These enzymes were initially purified and characterized from *B. subtilis* (*7*−*12*).

CwlC amidase, an *N*-acetylmuramoyl-L-alanine amidase, is secreted from sporulating *B. subtilis* cells (*13*) and can hydrolyze vegetative cell walls and spore peptidoglycan in vitro. Furthermore, a *cwlB cwlC* double mutant is resistant to mother-cell lysis during the late stage of sporulation (*13*). CwlC is a 27 kDa protein composed of 255 amino acids and consists of modular structural components comprising an N-terminal catalytic domain and two C-terminal tandem repeat sequences (Figure 1A,B). Application of the cell wall hydrolysis assay using a C-terminal repeat truncation mutant of CwlM, a homologous *Bacillus* enzyme whose sequence is 72% identical to that of CwlC, indicated that cell wall preference was impaired (*14*), and that the CwlC C-terminal repeats were required for efficient catalytic activity (*15*). These findings implied that the C-terminal repeat sequences play an important role in peptidoglycan binding. The Pfam database indicated that the C-terminal repeat sequences belong to a "sporulation-related repeat" family (pfam05036) (*16*), one of a conserved sequence family. This repeat is found in a tandem manner in many proteins involved in sporulation and cell division. However, direct biochemical data showing an interaction between peptidoglycan and the repeat have not been published.

In this study, we present the solution structure of the C-terminal repeat sequences, designated CwlCr, consisting of repeat 1 (residues 184−219) and repeat 2 (residues 120−255), by heteronuclear multidimensional NMR. On the basis of the well-defined structure, detailed structural pictures were described. The peptidoglycan interaction sites of CwlCr were identified using NMR, representing the first report showing that the sporulation-related repeats directly bind peptidoglycan itself. Furthermore, the structure of the circularly permuted repeat mutant was also characterized by NMR. Interestingly, the mutant adopted a similar folded structure, implying that the hydrophobic residues conserved between the repeats were key residues involved in folding.

[†] This work was supported in part by Grants-in-Aid for Scientific Research and 21st Century COE Research from MEXT (the Ministry of Education, Culture, Sports, Science, and Technology) of Japan.

[‡] The atomic coordinates of the ensemble of CwlCr structures have been deposited in the Protein Data Bank as entry 1X60.

* To whom correspondence should be addressed. Telephone: +81-743-72-5571. Fax: +81-743-72-5579. E-mail: kojima@bs.naist.jp.

[§] Nara Institute of Science and Technology.

[∥] Shinshu University.

10.1021/bi050624n CCC: $30.25
Published on Web 07/08/2005

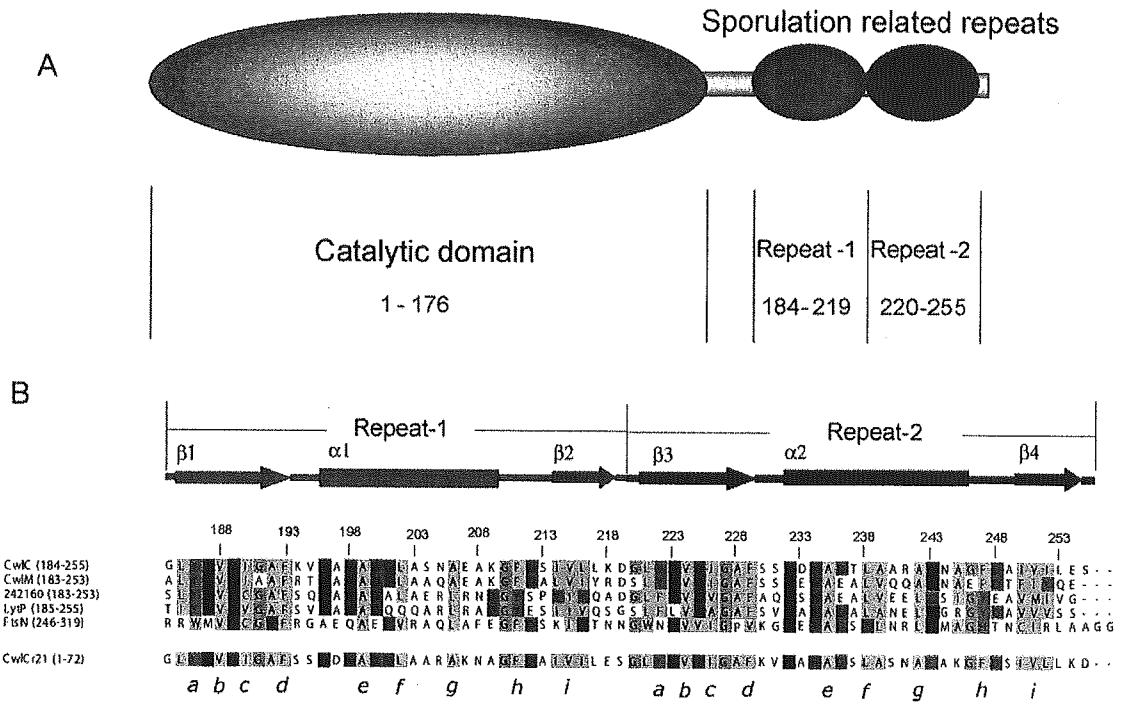

FIGURE 1: (A) Domain structure of CwlC. N-Terminal catalytic domain and C-terminal repeat sequences are schematically indicated. (B) Multiple-sequence alignment of sporulation-related repeats of cell wall lytic amidase. The secondary structure elements of CwlCr are shown schematically at the top. *a*−*i* denote the conserved hydrophobic residues. CwlCr, CwlM, 242160, LytP, and FtsN represent partial sequences of *B. subtilis* CwlC, *B. subtilis* CwlM, *Bacillus halodurans* C-125 sporulation mother cell wall hydrolase (NCBI accession number NP_242160), *Bacillus* sp. LytP, and *E. coli* FtsN, respectively. The first and last sequence numbers are indicated in parentheses. The repeat sequence of CwlCr21(1−72) is swapped, and residues 1−36 and 37−72 correspond to residues 220−255 and 184−219 of the wild type, respectively. Sequence alignment was initially obtained from a BLAST database search, realigned using ClustalW (*54*), and annotated using JALVIEW (*55*).

EXPERIMENTAL PROCEDURES

Sample Preparation. CwlCr was expressed in *Escherichia coli* M15 harboring a plasmid encoding CwlCr. Uniform labeling of proteins with ^{15}N or ^{15}N and ^{13}C was achieved using M9 minimal medium containing $^{15}NH_4Cl$ and [$^{13}C_6$]-glucose as the sole sources of nitrogen and carbon, respectively. Cells were grown at 37 °C, and protein expression was induced using isopropyl 1-thio-β-D-galactopyranoside when the A_{660} was 0.5. Cells were harvested 4 h following induction. Harvested wet cells were resuspended in 50 mM HEPES buffer (pH 7.5) containing 400 mM KCl and 0.1 mM EDTA. The suspension was lysed by sonication and ultracentrifuged, and the supernatant was loaded onto DEAE-Sepharose. The flow-through fraction was collected and purified using a Hitrap chelating column (Amersham Biosciences), charged with Ni ions, and eluted stepwise using imidazole. The hexahistidine tag was removed by specific cleavage using enterokinase. The protein was further purified by being passed through a Hitrap-S cation-exchange column (Amersham Biosciences). The homogeneity and identity of the purified protein were examined by SDS−PAGE and N-terminal analysis (M492 Perkin-Elmer), respectively. Protein concentrations were estimated using the calculated molar absorption coefficient at 280 nm ($\epsilon_{280} = 2.68 \times 10^3$ M^{-1} cm^{-1}). The expression and purification of the circularly permuted repeat mutant, CwlCr21, were performed as described above.

NMR Spectroscopy and Determination of the Structure of CwlCr. Purified CwlCr was dissolved in 50 mM potassium phosphate buffer (pH 6.5) containing 20 mM KCl and 0.1 mM EDTA in either a 95% H_2O/5% ^2H_2O mixture or 99.8% ^2H_2O. The final concentration of the protein was 1.7 mM. NMR spectra were acquired at 30 °C on a Bruker AVANCE 500 instrument equipped with a cryogenic probe and a Bruker DRX800 NMR spectrometer. Chemical shifts were referenced to 4,4-dimethyl-4-silapentane-1-sulfonate (DSS). For the purposes of collecting residual dipolar coupling restraints, nonionic liquid crystalline medium was used, consisting of 50 mM potassium phosphate buffer (pH 6.9), 20 mM KCl, 0.1 mM EDTA, 10% ^2H_2O, and a 5% $C_{12}E_5$PEG [*n*-dodecyl penta(ethylene glycol)]/hexanol mixture with a surfactant-

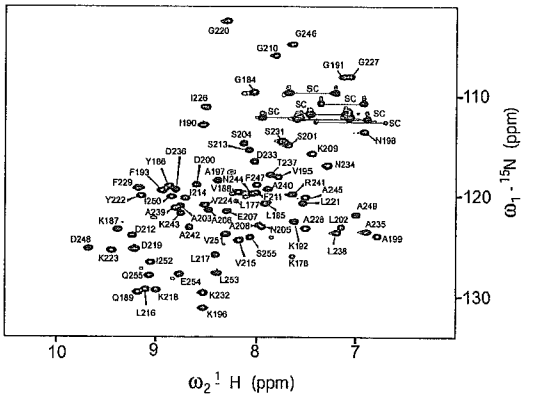

FIGURE 2: $^1H-^{15}N$ HSQC spectrum of CwlCr. The spectrum was obtained with 1.7 mM CwlCr at pH 6.5 and 30 °C. Assignments of the backbone amide groups are labeled. The SC label indicates side chain peaks of asparagine or glutamine residues.

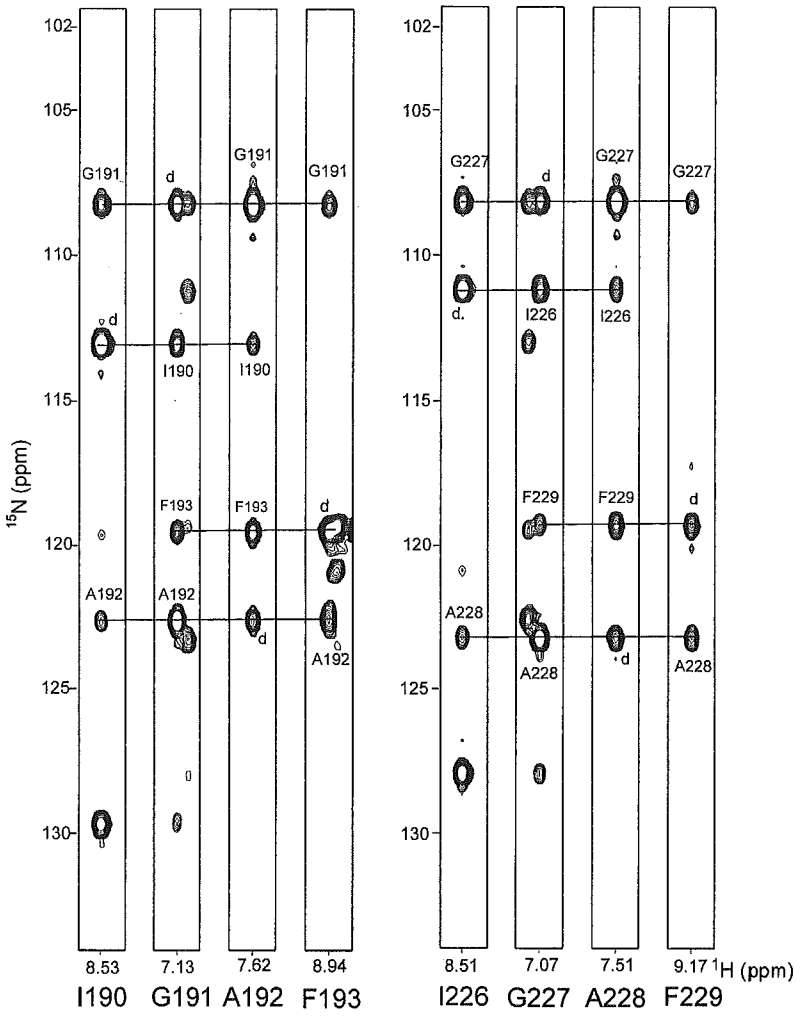

FIGURE 3: Selected $\omega_3(^1H)/\omega_1(^{15}N)$ strips from a 3D (H)N(CO-TOCSY)NH spectrum of CwlCr. The spectrum was acquired on a Bruker Avance 500 spectrometer equipped with a Cryogenic probe over the course of 30 h using a 1.7 mM solution of ^{13}C- and ^{15}N-labeled CwlCr at pH 6.9 and 30 °C. The strips are taken from slices at the backbone amide ^{15}N (F_2) frequency of each residue ranging from I190 to F193 (left) and from I226 to F229 (right). The experiment correlates the amide ^1H (F_3) and ^{15}N (F_2) chemical shift of each residue to the ^{15}N (F_1) chemical shift of the neighboring two or more residues in a relay manner. Sequential connectivity is shown by solid horizontal lines, and diagonal peaks are denoted with d.

to-alcohol ratio of 0.96 (*17*). This medium induced a deuterium splitting of ~15 Hz on the AVANCE 500 instrument. All multidimensional NMR spectra were acquired in a phase sensitive mode employing a States−TPPI or Rance−Kay method (*18*). The water flip-back method (*19*) was applied in several experiments that use amide proton magnetization. Shifted sine-bell window functions were applied to the NMR data prior to zero-filling and Fourier transformation. Mirror-image or forward−backward linear prediction was also used. All spectra were processed with the NMRPipe package (*20*), and analyzed using Sparky (*21*). ^1H, ^{13}C, and ^{15}N assignments were mainly obtained from standard multidimensional NMR methods (*22*, *23*), HNCACB, HN(CO)CACB, HN(CA)CO, and HNCO for main chain assignments and C(CO)NH, H(CCO)NH, HCCH-TOCSY, and four-dimensional (4D) HC(CO)NH (*24*) for side chain assignments. Any ambiguity relating to the sequential assignments was solved by a (H)N(CO-TOCSY)NH experiment (*25*). This experiment was slightly modified from the original sequence, wherein the first INEPT polarization transfer period (^{15}N to $^{13}C'$) was set to 54 ms, rather than the original 108 ms, since long delays caused significant sensitivity loss for CwlCr. Consequently, the adiabatic decoupling scheme for the aliphatic region was converted to simple decoupling using a Gaussian-cascade 3 pulse. The methyl groups of all Leu and Val residues were assigned in a stereospecific manner using a $^{13}C-^1H$ constant time HSQC spectrum of a randomly 15% ^{13}C-enriched protein sample (*26*). Most of the aromatic ^1H resonances were assigned by two-dimensional (2D) NOESY[1] on an unlabeled protein sample. Hydrogen bond restraints were derived from $^{h3}J_{NC'}$ couplings observed in the $^{h3}J_{NC'}$HNCO experiment (*27*, *28*). Interproton distances were derived from 2D NOESY, three-dimensional (3D) ^{15}N-edited NOESY-HSQC, 4D $^{13}C/^{15}N$-edited HMQC-NOESY-HSQC, and 3D ^{13}C-edited NOESY-HSQC spectra (*22*). Backbone dihedral angles were evaluated from vicinal coupling constants ($^3J_{HNHA}$) obtained from an HNHA experiment (*22*). Additionally, dihedral ϕ and ψ

[1] Abbreviations: NOE, nuclear Overhauser effect; NOESY, NOE spectroscopy; TOCSY, total correlation spectroscopy; HSQC, heteronuclear single-quantum correlation spectroscopy; rms, root-mean-square.